A

Thesis

on

Low temperature synthesis and characterization of carbon nanospheres from saccharides

Submitted in the fulfilment of the partial requirements for the award of degree of

Master of Science
in
Physics
(2015-2017)

submitted by

Rajpal Kour
(301504026)

Under the guidance of

Dr. Loveleen Kaur Brar
(Assistant Professor)

SCHOOL OF PHYSICS AND MATERIALS SCIENCE

THAPAR UNIVERSITY

PATIALA – 147004

July 2017

Dedicated to

My

Loving family

CERTIFICATE

This is to certify that this thesis entitled **Low temperature synthesis and characterization of carbon nanospheres from saccharides** is submitted by **Ms. Rajpal Kour** (Roll. No. 301504026) in the fulfilment of the partial requirement for the award of degree of Master in Science in Physics from School of Physics and Materials Science, Thapar University, Patiala (Punjab), India. It is an exclusive record of candidate's own research under the supervision of **Dr. Loveleen Kaur Brar**. This thesis in part or full has not been submitted in any other institute for award of such kind of degree.

Rajpal Kour

Date: 21 August, 2017

Place: Thapar university, Patiala.

Rajpal Kour

(301504026)

Dr. Loveleen Kaur Brar

(Assistant Professor)

School of Physics and Materials Science

Thapar University, Patiala-147004

ACKNOWLEDGMENT

I am submitting my thesis for the fulfilment of my 'M.Sc.' degree. This work would not have been accomplished without the help, support and guidance of a large number of people. I express my deep gratitude and respect to my supervisor **Dr. Loveleen Kaur Brar** (Assistant Professor, School of Physics and Materials Science) for her strong motivation, trust and constant encouragement during the course of work. I thank her for her great patience, constructive criticism and for giving me the opportunity to undertake this project.

I would like to thank to **Mr. O. P. Pandey** (Senior Professor and Dean R & SP, School of physics and materials science) for permitting me to use the facilities of his lab. Without his active support, it would have been not possible to carry out the experimental work.

I also express my heartiest gratitude to **Dr. Manoj Kumar Sharma** (Head and Professor, School of physics and materials science) for his support throughout the period and all the members of School of Physics and Materials Science for their help and suggestions at different stages of this work.

The meaning of my life and work is incomplete without paying regards to my loving family whose blessings and continuous encouragement have shown me the path to achieve my goals.

I would like to thank to **Mr. Aayush Gupta, Mr. Savidh Khan, Ms. Ruby Priya Rana, Ms. Raveena Chaudhary, Ms. Taranpreet Kaur Sandhu, Mr. Varun Singhal, Mr. Amit Singh Vig, Mr. Ghanshyam Mourya, Mr. Pardeep Bhatia, Ms. Era Gaba and Mr. Inderpreet Singh** for their moral support, patience, love and kindness.

Last but not the least I express my love and respect to my parents, my brother **Mr. Ravinder Singh** and my friend **Ms. Neha Chandel** for their love, support, motivation, trust and constant co-operation whenever I required.

And above all, I pay my regards to the Almighty Waheguru for his blessings.

Rajpal Kour

Rajpal Kour

CONTENTS

Sr. No.			Page No.
		Certificate	iii
		Acknowledgement	iv
		List of figures	vii
		List of tables	ix
		Abbreviations	x
		Abstract	xi
CHAPTER 1:		**INTRODUCTION**	**1-5**
1.1		Carbon nanospheres	1
1.2		Formation and structure of carbon nanospheres	2
1.3		Properties of carbon nanospheres	4
1.4		Applications of carbon nanospheres	4
1.5		References	5
CHAPTER 2:		**LITERATURE REVIEW**	**6-11**
2.1		Hydrothermal method	6
2.2		Pyrolysis method	9
2.3		Chemical vapour deposition method	9
2.4		Solvothermal method	10
2.5		Composite-molten-salt method	10
2.6		References	11
CHAPTER 3:		**MATERIALS AND METHODS**	**12-23**
3.1		Synthesis of carbon nanospheres	12
3.2		Structure and chemical formula of saccharide	13
	3.2.1	Sucrose	13
	3.2.2	Glucose	13
	3.2.3	Xylose	14
3.3		Characterizations	14
	3.3.1	X-Ray Diffraction (XRD)	14

3.3.2 Scanning Electron Microscope (SEM) 15
3.3.3 Field Emission Scanning Electron Microscope (FE-SEM) 16
3.3.4 Transmission Electron Microscope (TEM) 17
3.3.5 UV-Visible (UV-Vis) Spectroscopy 18
3.3.6 Fourier Transform Infrared Spectroscopy (FT-IR) 19
3.3.7 Dynamic light scattering (DLS) 19
3.3.8 Thermo gravimetric (TG) Analysis 20
3.3.9 Energy dispersive X-ray spectroscopy (EDX) 21
3.3.10 Inductively Coupled Plasma Mass Spectrometry (ICP) 21
3.3.11 Photo Catalytic Activity 21
3.4 References 23
CHAPTER 4: RESULTS AND DISCUSSION 24-37
4.1 Sample synthesis optimization 24
4.2 Mono-dispersed CNSs synthesis from sucrose 25
4.3 Effect of saccharide 30
4.4 Study of size distribution profile in the solution 32
4.5 TG analysis 33
4.6 Determination of impurity in CNSs samples 34
4.7 Photo-catalytic Activity 35
4.8 References 37
CHAPTER 5: CONCLUSIONS AND FUTURE SCOPE 38
5.1 Conclusions 38
5.2 Future scope 38

List of figures **Page No.**

CHAPTER 1: INTRODUCTION

Figure 1.1	(a) SEM image of CNSs	2
	(b) Open edges at the surface of carbon sphere	2
Figure 1.2	The arrangement of graphite layers in different forms to make CNSs	2
Figure 1.3	A diagram of spiral shell development from nucleation of pentagonal rings (a) Pentagonal rings (b) shell growth of quasi-icosahedral (c) Development of spiral shell (d) Synthesis of a big carbon sphere	3
Figure 1.4	A diagram representing the effect of (a) Hexagonal (b) Pentagonal (c) Heptagonal carbon rings on the curvature of carbon flakes	3

CHAPTER 3: MATERIALS AND METHODS

Figure 3.1	Typical flow chart showing the process for synthesis and characterization of CNSs	12
Figure 3.2	Crystal structure of sucrose	13
Figure 3.3	Crystal structure of glucose	13
Figure 3.4	Crystal structure of xylose	14
Figure 3.5	Diffraction of X-ray by planes of atom	15
Figure 3.6	Schematic illustration of Scanning electron microscope	15
Figure 3.7	Schematic of Field emission scanning electron microscope	16
Figure 3.8	Transmission electron microscope	17
Figure 3.9	UV-Visible spectrophotometer set up	18
Figure 3.10	Schematic illustration of FTIR system	19
Figure 3.11	Schematic of Dynamic light scattering	20
Figure 3.12	Thermo gravimetric analysis	20

CHAPTER 4: RESULTS AND DISCUSSION

Figure 4.1	SEM images showing the effect of synthesis time on the obtained product (a) 1 h (b) 5 h (c) 8 h (d) 18 h	24
Figure 4.2	XRD pattern of synthesized CNSs (sample SC04)	25
Figure 4.3	SEM/FE-SEM images of CNSs showing uniform and spherical morphology of CNSs for SC01, SC02, SC03, SC05 and SC06 (a-f)	26
Figure 4.4	(a) Particle size distribution of SC04 sample. (b) Particle size variation of CNSs with concentration. (Y-axis of the graph has been plotted in log to show the small size data clearly)	28
Figure 4.5	(a) TEM image for single CNS and (b) HR-TEM image for CNS showing {006} plane.	28
Figure 4.6	(a) The UV-Vis data obtained for the SC06 (b) Tauc plot for SC06	29
Figure 4.7	FT-IR spectra of synthesized CNSs for SC05, GL01 and XL01.	29
Figure 4.8	(a-b) TEM images of CNSs of GL01 and XL01	30
Figure 4.9	(a-b) FE-SEM images of CNSs of GL01 and XL01.	31
Figure 4.10	Particle size variation of CNSs with saccharides.	32
Figure 4.11	Particle size distribution graph for SC05.	33
Figure 4.12	TG plot of synthesized CNSs for SC04.	34
Figure 4.13	EDAX spectrum of CNS of SC04	35
Figure 4.14	Absorption spectra of degradation of MB under (a) visible source (b) UV source	35
Figure 4.15	Degradation of MB with time in the presence of UV and Visible light	36

List of tables **Page No.**

CHAPTER 4: RESULTS AND DISCUSSION

Table 4.1	Details of CNSs samples obtained for different synthesis times	25
Table 4.2	Details of monodispersed CNSs samples synthesized in present study. All the samples have been obtained by soaking the autoclave for 8 h at 180 °C.	27
Table 4.3	Represents the IR peak and the corresponding functional group.	30
Table 4.4	Represents the concentration and size distribution of various samples	33

List of abbreviations

CNSs	Carbon nanospheres
XRD	X-Ray diffraction
SEM	Scanning electron microscope
FE-SEM	Field emission scanning electron microscope
TEM	Transmission electron microscope
HR-TEM	High resolution transmission electron microscope
FT-IR	Fourier transform infrared spectroscopy
EDX	Energy dispersive X-ray spectroscopy
DLS	Dynamic light scattering
UV-Vis	Ultraviolet visible spectroscopy
TGA	Thermo gravimetric analysis
ICP	Inductively coupled plasma mass spectroscopy
MB	Methylene blue

ABSTRACT

Nanostructures have sizes that lie between macroscopic and molecular structures. Carbon nanostructures attract large attention due to their attractive properties which can be modified. They find applications in diverse fields such as electrodes, sensors, catalyst support etc. Among these structures, carbon nanospheres (CNSs) are of great interest in scientific research due of their properties such as good electrical conductivity, high surface area, uniformity and thermal stability. They have been used in many applications such as Li-ion batteries, material reinforcement, fuel cells etc. In the present study the mono-dispersed carbon nanospheres were synthesized by hydrothermal process using various saccharide solutions – sucrose, glucose, and xylose. The saccharide solution in required concentration was sealed in a steel autoclave and heated at 180 °C for the prescribed time. The as-synthesized CNSs were characterized using X-Ray diffraction (XRD), Fourier transform infrared (FTIR) spectroscopy, Scanning electron microscope (SEM), Transmission electron microscope (TEM), UV-Visible spectroscopy, Thermo-gravimetry (TG) etc. for their structural, optical, thermal and other important properties. The size of the CNSs decreases with the saccharide solution concentration with smaller concentrations having more drastic effect. The CNSs produced from the present method typically have an average size in the range of 1500 – 15nm having smooth surfaces. Xylose gives the smallest CNSs. The CNSs were amorphous in nature. Samples show direct band gap which changes with the size of CNSs. This makes the synthesized samples viable for the photo catalytic applications in UV as well as visible region. The application of the synthesized CNSs as photo catalyst for organic waste degradation has been confirmed by degradation of methylene blue (MB) dye in the presence of UV and visible light. The degradation efficiency is more in visible light.

CHAPTER 1

INTRODUCTION

1.1 Carbon nanospheres

The discovery of carbon nanostructures have attracted the research in modern era due to attractive properties which can be modified controlled ways. Carbon nanostructures are widely used in various fields such as catalysis, material reinforcement, hydrogen storage and electronics [1-6]. These materials have multiple interesting and useful applications.

Carbon shows the property of catenation. It can make bond with other atoms (O, H, S, N, C etc.). This property leads to formation of many structures which are useful in many fields [7]. The applications and advantages of carbon materials, synthesis and characterization have attracted the modern research. These structures have dangling bonds present on their surface which have good physical strength. The presence of dangling bonds provides functional groups on the surface of the carbon materials. This property makes them useful for Li-ion batteries and catalysis. Fullerenes were discovered in 1985. Fullerene is a molecular carbon which exists in many shapes like hollow sphere, ellipsoid and tube. The other carbon structures are nanofibers, nanotubes and nanospheres which have size in the range from 0.4-500nm. These are formed by pairing of pentagonal, heptagonal and hexagonal shaped carbon rings.

Among the carbon nano materials, spherical carbon materials have attracted great attention because of their uniform size, high surface area and physicochemical properties. These spherical carbon structures have been given different names due to their different sizes like carbon onions, carbon black etc [8]. The nano size and morphology leads them to show different properties than the bulk carbon materials. This may be attributed due to high surface to volume ratio, quantum confinement effect. Our main focus is to synthesize the carbon nanospheres (CNSs) by hydrothermal process [9].

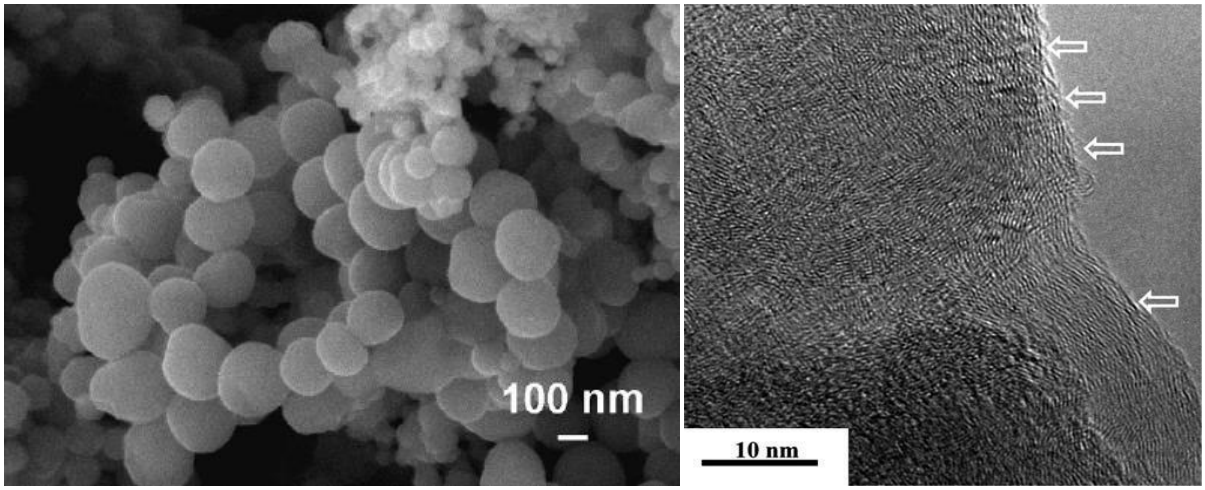

Figure 1.1: (a) SEM image of CNSs and (b) open edges at the surface of Carbon Sphere [10].

1.2 Formation and structure of carbon nanospheres

With the help of suitable synthesis process and controllable parameters, the nano sized and spherical shape carbon materials can be obtained. The spherical structures are formed when the fullerene rings get attached into each-other. Many open edges are created at the surface of carbon spheres. The nature of carbon structures can be graphitic or non-graphitic. The graphitic sheets have unclosed shells and make dangling bonds on the surface of carbon structures [11].

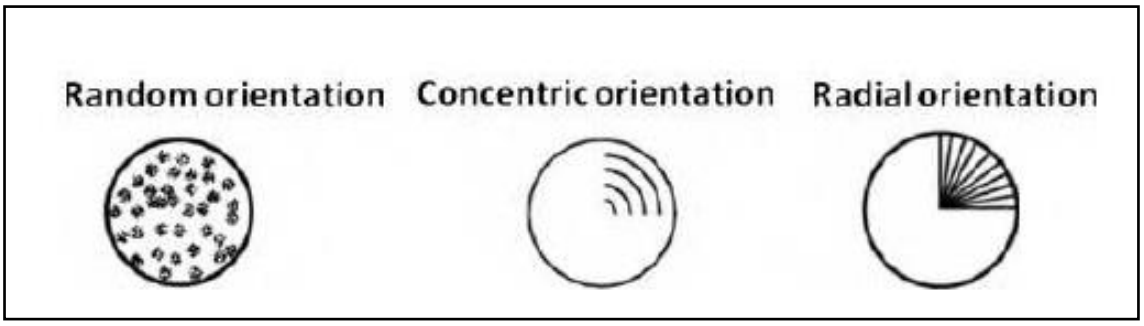

Figure 1.2: The arrangement of graphite layers in different forms to make CNSs [8].

For the synthesis of carbon structures many models have been proposed. The most studied model in the literature is the nucleation of pentagonal rings of carbon atoms. These rings attach with each-other results in the formation of spiral shell growth as shown in the following figure 1.3.

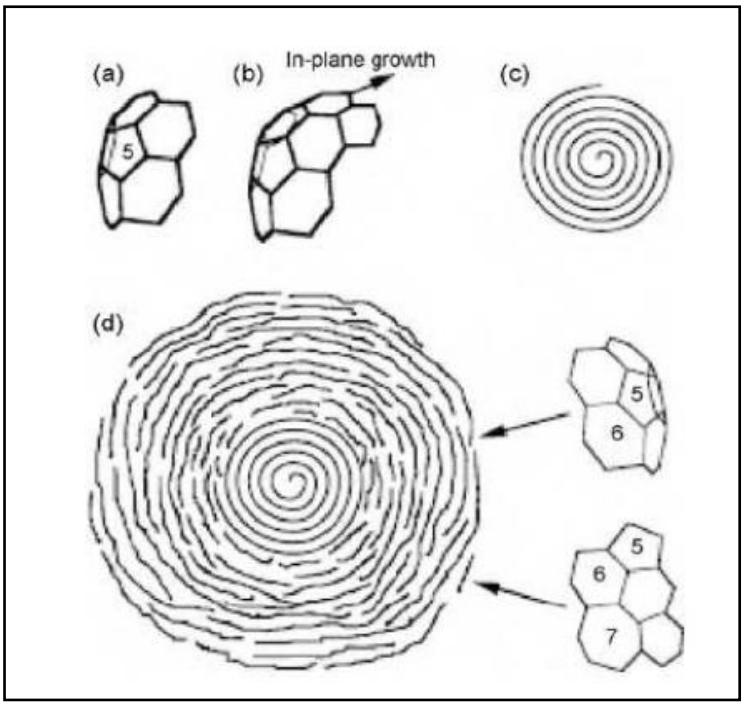

Figure.1.3: A diagram of spiral shell development from nucleation of pentagonal rings (a) Pentagonal nucleation (b) shell growth of quasi-icosahedral (c) Development of spiral shell (d) Synthesis of a big carbon sphere. [12]

A continuous curved sheet can be observed on the surface of carbon spheres. The carbon structures greater than 10nm in size have graphite layers on their surface. The carbon rings are essential and useful to obtain this curvature [13].

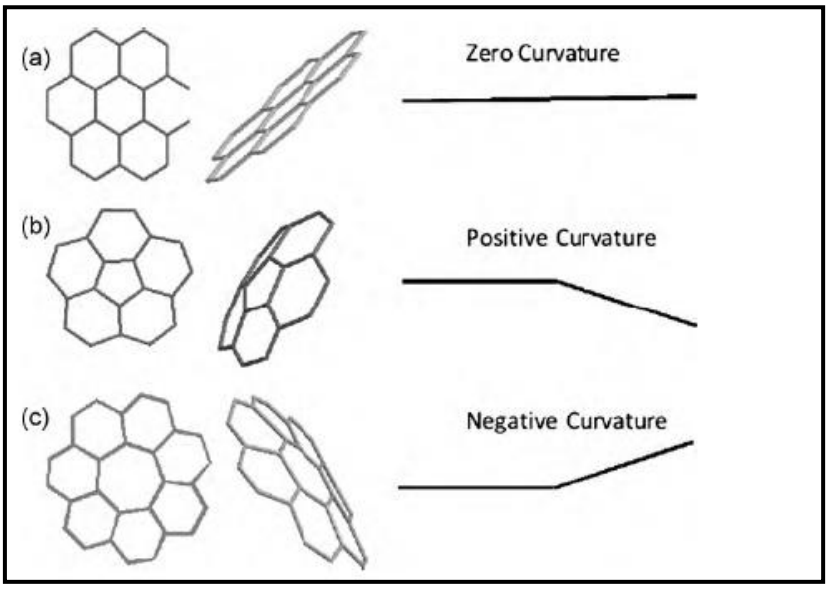

Figure 1.4: A diagram representing the effect of (a) Hexagonal, (b) Pentagonal and (c) Heptagonal carbon rings on the curvature of carbon flakes [13].

1.3 PROPERTIES OF CNSs

Carbonaceous materials are useful in many fields and industries due to their properties such as: [14-19]

- Good electrical conductivity (~ 45 S/m)
- High surface area (~3,022 m^2g^{-1})
- Porosity (>80%)
- Tailored specific surface chemistry
- Uniformity (~ 95%)
- High thermal stability (~ 500 ˚C)
- Large packing density

1.4 APPLICATIONS OF CNSs

Carbon nano spheres have wide range of applications and improvement of these applications depends on the ability of controlling the size, band gap and surface properties of CNSs [20-22].

- Electrode for super capacitors
- Anode in secondary lithium batteries
- Absorbent
- Sensors
- Material reinforcement
- Capsules for magnetic nano particles
- Template for hollow structures
- Catalyst for direct methanol fuel cells
- Refinement of aqueous solutions
- Hydrogen storage and electronics

References

1. J. Chen, N. Xia, T. Zhou, S. Tan, F. Jiang, D. Yuan, Int. J. Electrochem. Sci. **4** (2009) 1063-1073.
2. Y. Z. Jin, Y.J. Kim, C. Gao, Y.Q. Zhu, A. Huczko, M. Endo, H.W. Kroto, Carbon **44** (2006) 724-729.
3. X. Sun, J. Lin, Chem. Eur. J. **12** (2006) 2039-2047.
4. Z. Wang, P. Xiao, N. He, Carbon **44** (2006) 3277-3284.
5. X. Song, P. Gunawan, R. Jiang, S. S. Leong, K. Wang, R. Xu, J. Hazard Mater. **194** (2011) 162-168.
6. Z. Wen, Q. Wang, Q. Zhang, J. Li, Electrochem. Commun. **9** (2007) 1867-1872.
7. H. W. Kroto, J.R. Heath, S.C. O' Brien, R.F. Curl, R.E. Smalley, Nature **318** (1985) 162-163.
8. A. Deshmukh, S. Mhlanga, N. Coville., Mat. Sci. Eng. R **70** (2010) 1-28.
9. M.H. Joula, M. Farbod, Appl. Surf. Sci. **347** (2015) 535-540.
10. A.N. Marquez, R. Romero, A. Romero, J.L. Valverde, J. Mater. Chem. **21** (2011) 1664-1672.
11. Z. Wang and Z. Kang, Philos. Mag. B **73** (1996) 905-929.
12. Z. Wang and Z. Kang, J. Phys. Chem. **100** (1996) 17725-17731.
13. Z. Wang, Z. Kang, J. Phy. Chem. **100** (1996) 5163-5165.
14. M. Sobkowicz, J. Dorgan, K. Gneshin, A. Herring and J. Mc Kinnon., Carbon **47** (2009) 622-629.
15. T. Thome, J. Colaux, J. Colomer, G. Bertoni and G. Terwagne, Mat. Chem. Phys. **103** (2007) 290-294.
16. V. Pol., Environ. Sci. Technol. **44** (2010) 4753-4759.
17. F. Xu, Z. Tang, S. Huang, L. Chem, Y. Liang, W. Mai, H. Zhong, R. Fu and D. Wu, Nature **6** (2015) 7221.
18. G. He, S. Evers, X. Liang, M. Cuisinier, A. Garsuch, L. F. Nazar, ACS Nano **7** (2013) 10920-10930.
19. G. Li, C. Guo, C. Sun, Z. Ju, L. Yang, L. Xu, Y. Qian, J. Phys. Chem. C **112** (2008) 1896.
20. R. Alcantara, F. Madrigal, P. Lavela, J. Tirado, J. Mateos, C. Zhecheva, Carbon **38** (2000) 1031-1041.
21. F. Zhang and H. Li, Mater. Chem. Phys. **98** (2006) 456-458.
22. S. Han, Y. Yun, K. Park, Y. Sung, T. Hyeon, Adv. Mat. **15** (2003) 1922-1925.

CHAPTER 2

LITERATURE REVIEW

Carbon nanospheres are used in many fields of application because of their large surface area and have become an interesting topic in scientific studies. An overview of different methods to prepare carbon nanospheres and their properties characterized by different techniques has been discussed in this chapter. Some methods available in literature to synthesize carbon spheres are as follows:

2.1 Hydrothermal method

Qiang et al. (2005) [1] synthesized carbon microspheres using hydrothermal process. Carbon microspheres were prepared by methylcellulose sol in a stainless steel autoclave by heating it on 400˚C for 6 h in an oven. The crystal structure of as-synthesized CNSs was analyzed by X-ray diffraction. A wide peak was observed at angle 26˚ which indicates the amorphous structure of CSs. The morphology, size and structure were characterized by scanning electron microscope (SEM) and transmission electron microscope (TEM). SEM micro images showed the formation of smooth CNSs having diameters in the range of 1-5μm and spherical morphology with chain like structure of CSs was presented by TEM.

Rongjing et al. (2008) [2] prepared monodispersed colloidal CNSs using microwave hydrothermal method by glucose solution. A self-assembly process was used to prepare gold nanoparticles (AuNPs) on the surface of colloidal CNSs. These colloidal carbon nanospheres (AuNPs) hybrid materials had good chemical stability and used as template for bio molecule deactivation and biosensor invention. The as-prepared CNSs were characterized to examine their chemical stability and biocompatibility. The FT-IR spectra showed the presence of C=O, C=C, C-OH and OH functional groups. The FE-SEM and TEM results represented the images of AuNP/C materials and colloidal CNSs of uniform size (250nm) and morphology. It was observed that these AuNP/C carbon spheres can be used for the formation of immunosensor to examine their feasibility in bio electro analysis.

Jingxing et al. (2009) [3] obtained monodispersed CNSs from glucose by hydrothermal technique without any catalyst. High specific area and mesoporous CNSs of nanometer size were prepared by melton KOH treatment.

The uniform and nano size CNSs were characterized by SEM where as solid structure and rough surface of carbon spheres were analyzed by TEM. The size of CSs was about 700-800 nm that was observed by SEM. The HR-TEM images showed 3 nm CNSs with 0.20 nm fringe spacing. The amorphous structure of CNSs was observed by XRD pattern. The peaks of O-H, C-H and C-O functional groups were analyzed by FT-IR on the surface of mesoporous CSs. These MCSs were used as electrode materials for super capacitors.

Minmin et al. (2009) [4] produced hollow CNSs by hydrothermal process without using template. In this procedure sodium alginate was mixed in DI water. The solution was sealed in a Teflon coated autoclave and then heated at 180˚C for 10 h. CNSs of size 100nm were obtained using alginate as reagent. TEM images showed the nano size spheres in the range of 70-120nm and uniform morphology. Because of poor crystallization the amorphous structure of carbon was obtained from XRD analysis. Several functional groups i.e. C=O, C=C, OH, C-OH and CHO were found on the surface of CNSs by FT-IR spectra. Cross linked hollow CNSs and changing morphology was characterized when the concentration of sucrose was changed from 0.1 to 0.5gm. As-prepared CNSs can be used in many fields like catalysts, storage and carriers.

Antonio et al. (2010) [5] obtained hollow CNSs of 100nm from hydrothermal process. The solution of glucose and sodium dodecyl sulphate was treated at 180˚C. The amorphous structure of CNSs due to low crystallinity was observed from broad peaks of XRD pattern. The D and G-bands of Raman spectra represents the graphitic layer structure of CNSs. TEM micrographs showed the hollow and solid CNSs. From SEM images it was observed that CNSs had spherical and uniform morphology. These hollow CNSs can be used in many fields like nanocomposites, fuel cells etc.

Ying et al. (2010) [6] synthesized mesoporous and nano size carbon spheres from a low concentration hydrothermal route. These carbon structures had large surface area and porosity which is useful in adsorption and can be used in super capacitors, lithium batteries and fuel cells. SEM results showed that these mesoporous CNSs had nanometre size and spherical shape. The isolated particles of size 140 nm were obtained from HRSEM and TEM images. At high temperature the cross-linking process of CNSs was observed and spherical morphology was obtained due to isotropic crystal growth.

Shaochun et al. (2012) [7] used hydrothermal process to obtain CNSs. In the typical hydrothermal process the sucrose solution was heated at 190˚C for 2-8 h in an

autoclave. The size, morphology and shape of CNSs were characterized by FESEM and TEM. From FESEM images it was noticed that the size of CNSs increases from 250-1200 nm with the increasing reaction time. The TEM images represented the formation of CNSs having size in the range of 8-10 nm.

Aled et al. (2014) [8] converted carbohydrates and raw lignocellulosic biomass into carbonaceous materials using hydrothermal process. The glucose solution was transferred in a steel autoclave and heated at temperature 160-180˚C into an oven. The size controlled carbon spheres (CSs) were obtained by changing the reaction time from 2-10 h. The size of CNSs was increased from 200-1500 nm with the reaction time. These CSs can be used in Li-ion batteries and electrodes for Li-S batteries.

Shashi et al. (2014) [9] produced imine-functionalized CNSs with plant extract from a single-step hydrothermal carbonization. The chemical properties of as-synthesized CNSs were characterized from different techniques. The size of peCNSs (0.5-3 μm) was determined with the varying concentration of plant extract. The FTIR spectrum showed the presence of C-H, C-O, C=C and imine functional groups. The nature of CSs was determined by Raman spectra and the amorphous carbon structure was obtained by XRD pattern. The adsorption-desorption process showed that the efficiency of peCNSs does not decreases after repetitive use and these CNSs can be potentially applied to uranium recovery from aqueous solutions.

Mohsan et al. (2015) [10] made monodispersed, high yield carbon nanospheres by hydrothermal process and their sizes were reduced by changing the concentration of initial solution. The sucrose solution was transferred in a steel autoclave and heated in an oven at 170^0C for 8h. The diameter of CNS was reduced to 100nm by post- annealing of 300nm CNSs at 435^0C for 30min. These CNSs had wide range of applications which depend on the size and surface properties.

The samples were characterized to examine the structure, size and properties of CNSs. The XRD pattern showed the low graphitization degree and disordered carbon structures. SEM images showed that the CNSs had good spherical shapes and smooth surfaces. IR spectroscopy (Infrared spectroscopy) showed that the surface functional group –OH increases with decreasing size of CNSs due to increase in their surface area.

Qiangu et al. (2015) [11] characterized CNSs prepared by hydrothermal carbonization of four different saccharides- sucrose, glucose, xylose and saccharide formed by pinewood. From SEM images it was observed that CNSs produced by xylose had small

size (80nm) and uniform shapes. While CNSs prepared from glucose (120-150nm) and sucrose (300-400nm) had non-uniform shapes. TEM images showed the images of long C-C chain structures prepared by sucrose and nano size CNSs of size 50-100nm derived from pine wood sugar solution. These CNSs with surface oxygen functional groups and nanometre size were used in hydrothermal carbon hybrid materials. These CNSs had potential to use in many applications.

2.2 Pyrolysis method

Hans et al. (2015) [12] prepared carbon nanospheres under nitrogen atmosphere by simple pyrolysis method. They used activated carbon as support, ferrocene as catalyst and cooking palm oil as renewable. The concentration of iron was changed to prepare nano size CNSs.

The change in size and morphology of carbon were observed by scanning electron microscope (SEM). It was that the density of CNSs increases with the increasing concentration of iron catalyst. The concentration of iron on the surface of carbon was determined by Energy dispersive X-ray spectroscopy (EDS). Amorphous structure of activated carbon was observed by XRD analysis.

Vinodkumar et al. (2015) [13] prepared CNSs by template free pyrolysis method. In this method a metal salt was added in sucrose. The decomposition of sucrose was done by heating it to make metal oxide particles. During the process of lithiation-delithiation it was observed that the as-synthesized CNSs had structural stability.

XRD pattern showed the amorphous structure of porous CNSs. The SEM and TEM images showed that temperature did not affect morphology and size of CNSs (100-2000 nm). The graphitic layers were observed from high resolution TEM (HR-TEM) images. The electrochemical performance of CNSs was explained due to the porosity and disordered crystal structure. These porous CNSs had higher charge potential and can be used in Li-ion batteries.

2.3 Chemical vapour deposition method

Antonio et al. (2010) [5] observed applications and properties of porous carbon spheres synthesized chemical vapour deposition method. The CNSs were obtained by the decomposition of acetylene over Co supported on a kaolin plate at 750˚C. These CSs had poor graphitization degree and diameters in the range of 2-10 μm.

The amorphous structure of CNSs was observed from broad peaks of XRD pattern because of low crystallinity. The graphitic layer structure of CNSs was observed from D and G-bands of Raman spectra. SEM images represented the uniform and spherical structure of CNSs. TEM micrographs showed the hollow and solid CNSs. These CNSs can be used in many areas such as catalysis, electrical devices and fuel cells.

Aled et al. (2014) [8] produced porous carbon spheres by chemical vapour deposition (CVD) method. In this method the high temperature treatment of carbon precursor was done to prepare hollow and solid carbon spheres. The presence of catalyst acted as nuclei for the formation of CNSs. The nano size CSs were obtained by changing the state of carrier gas. The sample was characterized to examine the morphology and topography of CNSs. the SEM and TEM images represented the hollow and narrow size CNSs having diameters in the range of 200 -400 nm. These CNSs can be used in Li-ion batteries and electrodes for Li-S and Li-air batteries.

2.4 Solvothermal method

Mani et al. (2015) [14] made CNSs by solvothermal route using acetone and Mg as a reducing agent. The samples were characterized by different techniques to examine the size, structure, stability and properties of CNSs. Photo catalytic activity was studied from the degradation of methylene blue in UV light in the presence of CNSs. The broad peaks obtained by XRD pattern showed the disordered carbon structure. SEM results represented the images of spherical, uniform and nano size CNSs of size 40-50 nm. TG/DTA analysis provides the thermal stability curve of CNSs. The band gap for direct transitions was calculated by UV-Vis spectra i.e. 3.54 eV.

2.5 Composite-molten-salt method

Xue et al. (2010) [15] used composite-molten-salt (CMS) method to prepare functional CNSs. The carbonization and dehydration of glucose was done at 200^0C without using any solvent. The SEM and TEM images showed the nano size (200nm) and solid structure of CNSs. The FT-IR spectrum showed the presence of –OH, C-H and C=C functional groups on the surface of CNSs. The D (diamond) and G (graphitic) bands of Raman spectra represented the band hybridisation of CNSs. CNSs prepared by this method had good electrochemical performance as compared to the other methods used to make CNSs.

References

1. Q. Wang, F. Cao, Q. Chen, C. Chen, Mater. Let. **59** (2005) 3738-3741.
2. B. R. Cui, C. Lin, J. shen, D. Gao, J. Zhu, H. Chen, Adv. Funct. Mater. **18** (2008) 2197-2204.
3. J. Chen, N. Xia, T. Zhou, S. Tan, F. Jiang, D. Yuan, Int. J. Electro chem. Sci. **4** (2009) 1063-1073.
4. M. Li, Q. Wu, M. Wen, J. Shi, Nanoscale Res Lett **4** (2009) 1365-1370.
5. A. Nieto-Marquez, R. Romero, A. Romero, J. L. Valverde, J. Mater. Chem. **21** (2011) 1664-1672.
6. Y. Fang, D. Gu, Y. Zou, Z. Wu, F. Li, R. che, Y. Deng, B. Tu, D. Zhao, Angew. Chem. Int. Ed. **49** (2010) 7987-7991.
7. S. Tang, S. Vongehr, X. Meng, Nanotechnology **23** (2012) 095 603 (11pp).
8. A. D. Roberts, X. Li, H. Zhang, Chem. Soc. Rev. **43** (2014) 4341.
9. S. P. Dubey, A. D. Dwivedi, M. Sillanpaa, Y. kwon, C. Lee, RSC Adv. **4** (2014) 46114.
10. M. H. Joula, M. Farbod, Appl. Surf. Sci. **347** (2015) 535-540.
11. Q. Yan, R. Li, H. Toghiani, Z. Cai, J. L. Zhang., T. R. Energy **1** (2015) 119-128.
12. H. Kristianto, C. D. Putra, A. A. Arie, M. Halim, J. K. Lee, Procedia chem. **16** (2015) 328-333.
13. V. Elacheri, C. Wang, M. J. O'Connell, C. K. Chan, V. G. Pol, J. Mater. chem. A **3** (2015) 9861.
14. M. Mahajan, G. Singla, K. Singh, O.P. Pandey, J. solid state chem. **232** (2015) 108-117.
15. X. Wang, C. Hu, Y. Xiong, X. He, Y. Xi, C. Xia, J. Nanosci Nanotechnol. 13 (2013) 933-6.

CHAPTER 3

MATERIALS AND METHODS

In this chapter sample preparation method and characterization techniques are discussed which were followed during the study of present investigations.

3.1 Synthesis of carbon nanospheres

Uniform and monodisperse carbon nanospheres (CNSs) were prepared by sucrose, glucose and xylose using hydrothermal process. The molecular structure and chemical formula of these saccharides is given in the section 3.2 of this chapter. The purity of saccharides which were used to synthesize the samples was ≥ 99%. All the chemicals were purchased from LOBA Chemie or SDFCL, India. DI water was taken from Millipore Q3 system having resistivity 18.2 MΩ to prepare the saccharide solution.

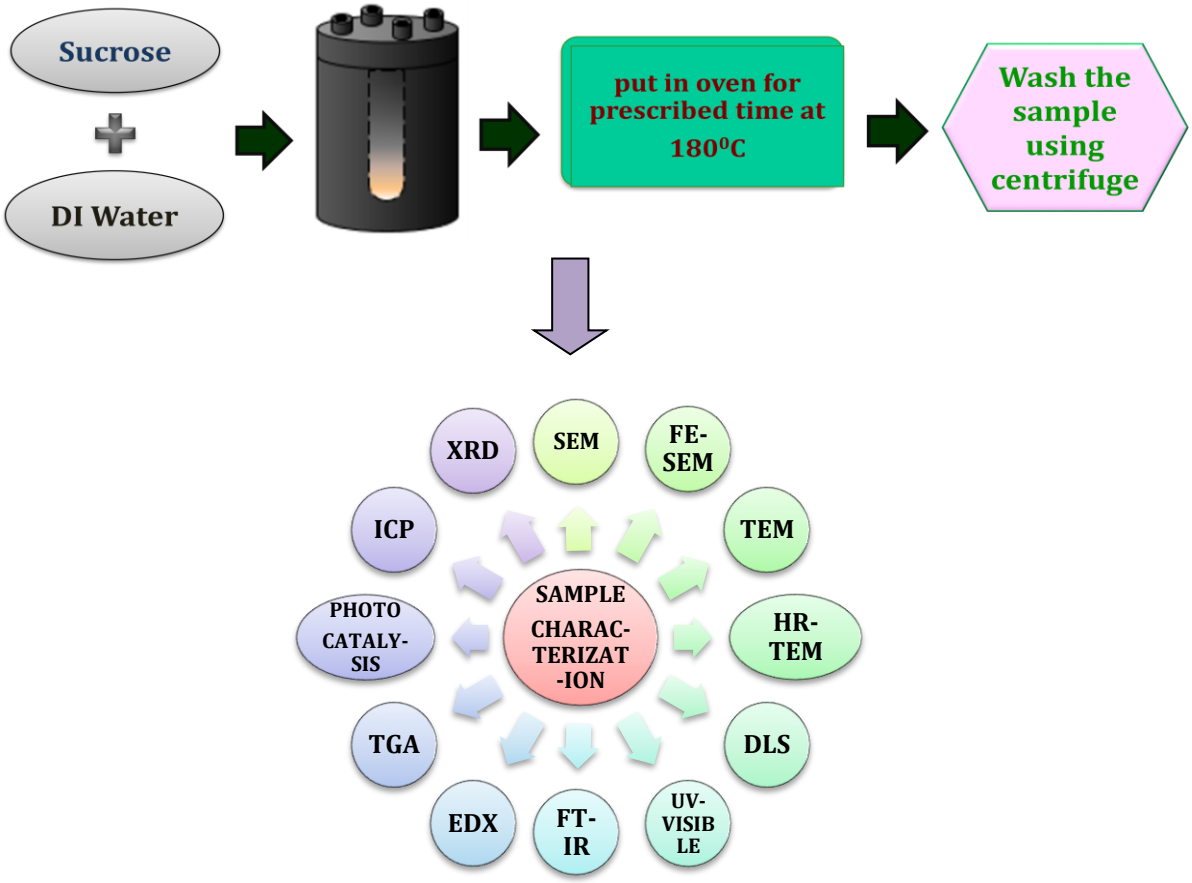

Figure 3.1: Typical flow chart showing the process for synthesis and characterizations of CNSs.

For each sample, the solution was prepared by dissolving the proper amount of saccharide in DI water. The solution was transferred into a 25ml specially designed steel autoclave. The autoclave was sealed properly and placed in an oven. The oven temperature was increased from room temperature to 180˚C and kept at this temperature for prescribed time. The autoclave was then allowed to cool down at room temperature naturally. The products were collected by using 10000 - 14000 rpm centrifuge and washed several times with DI water [1]. The information related with preparation and characterizations are given in the flow chart (figure 3.1)

3.2 Structure and chemical formula of saccharides

3.2.1 Sucrose:

Chemical formula- $C_{12}H_{22}O_{11}$

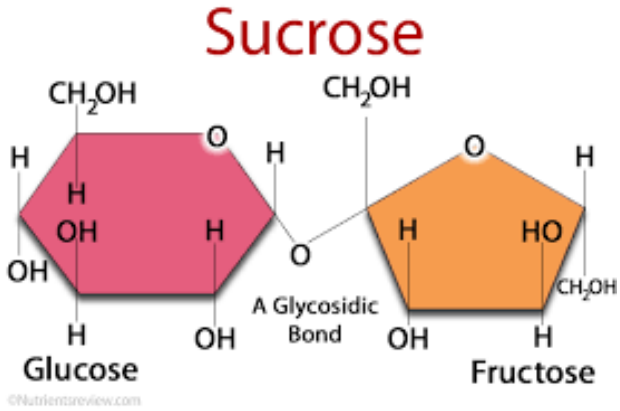

Figure 3.2: Crystal structure of sucrose.

3.2.2 Glucose:

Chemical formula- $C_6H_{12}O_6$

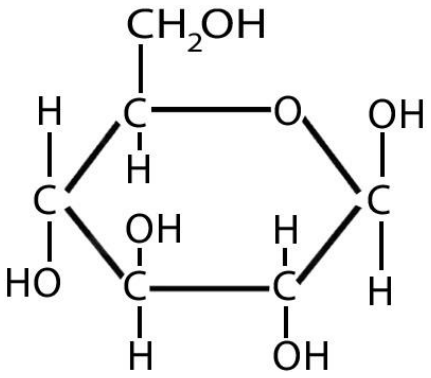

Figure 3.3: Crystal structure of glucose.

3.2.3 Xylose:

Chemical formula- $C_5H_{10}O_5$

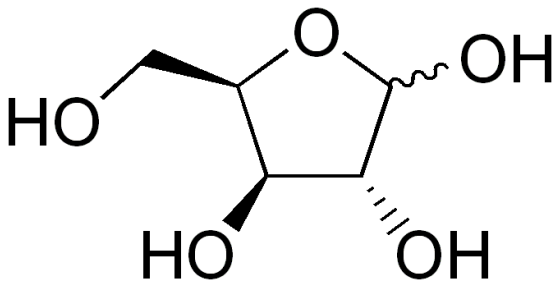

Figure 3.4: Crystal structure of xylose.

3.3 Characterizations:

Different characterizations must be performed on the samples to examine their properties. The X-ray diffraction technique has been done to characterize the structure of CNSPs. The size, morphology, topography was observed by Scanning electron microscope (SEM), Field emission scanning electron microscope (FE-SEM) and high resolution transmission electron microscope (HR-TEM). The particle size distribution profile was analyzed by dynamic light scattering (DLS). The presence of functional groups on the surface of CNSPs was observed by Fourier transform infrared spectroscopy (FT-IR). The band gap was calculated by UV-Visible spectroscopy. The particulars of these techniques are as follows:

3.3.1. X-ray diffraction (XRD)

XRD analysis is a non-destructive technique to determine the structure of crystalline materials, their disordering and crystallite size. As shown in figure 3.5 X-rays incident on the crystal and makes an angle 'θ' with respect to plane of atoms and the separation distance is d. The relation between the constructive interference of rays is determined by Bragg's law, which is given by:

$$2d \sin\theta = n\lambda \qquad (3.1)$$

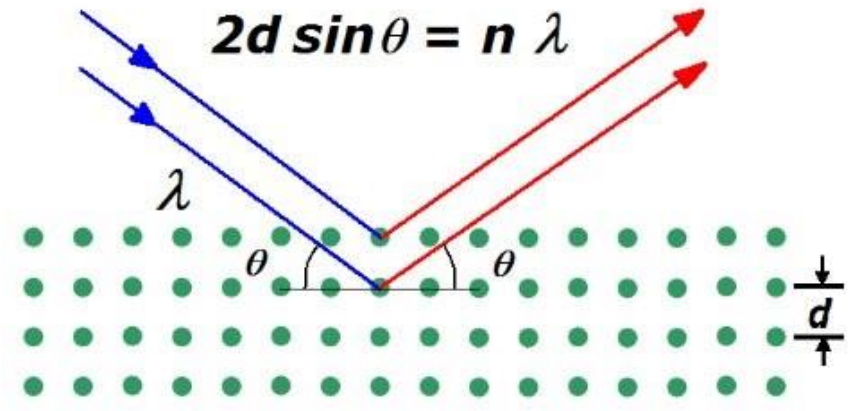

Figure 3.5: Diffraction of X-ray by planes of atom [2].

The XRD pattern was recorded at room temperature using *PANalytical X'Pert PRO* diffractometer to find the crystal structure of carbon nanospheres. The 2θ values were taken in the range of 10˚ to 80˚ for XRD pattern.

3.3.2 Scanning Electron Microscope (SEM):

SEM is a common characterization technique that produces images of a sample by scanning it with focusing a narrow beam of electrons emitted from the microscope onto a point on the sample. The information about the topography and composition of the sample can be obtained by producing various signals of electrons that interact with atoms in the sample. Figure 3.6 shows the schematic diagram of SEM.

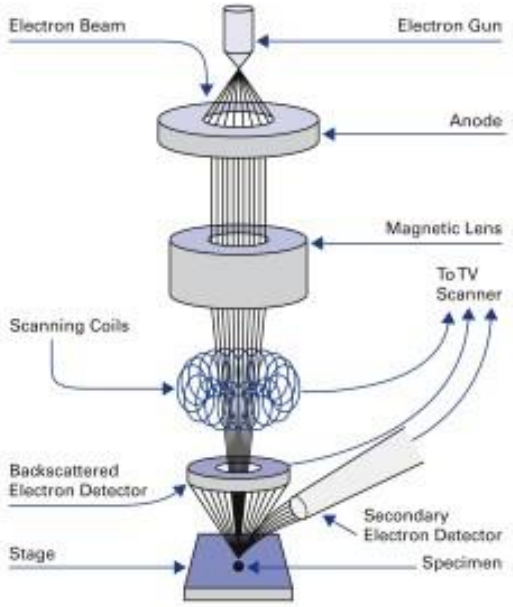

Figure 3.6: Schematic illustration of Scanning Electron Microscope [3].

Electron microscope images at low and high magnification were taken with a *JEOL JSM-6510LV* scanning electron microscope at 15kV. A drop of the CNSs solution was placed on carbon tape (applied on the SEM sample stub), dried under a lamp and finally heated in oven at 55˚C to remove the moisture. The samples were coated with gold after they dried completely.

3.3.3. Field Emission Scanning Electron Microscope (FE-SEM):

In a field emission SEM field emission source (gun) is used to generate the electrons. This FE gun emits the electron from a very small area and has low cross over diameter. This gun is more coherent and energy spread is very low. The beam passes through electromagnetic lenses focussing onto the sample. The object is scanned by electrons according to pattern. FESEM produces clear, low voltage and high quality images. FE-SEM is used to determine very small topographic details on the surface of an object. A schematic diagram of near field emission scanning electron microscope is shown in figure 3.7.

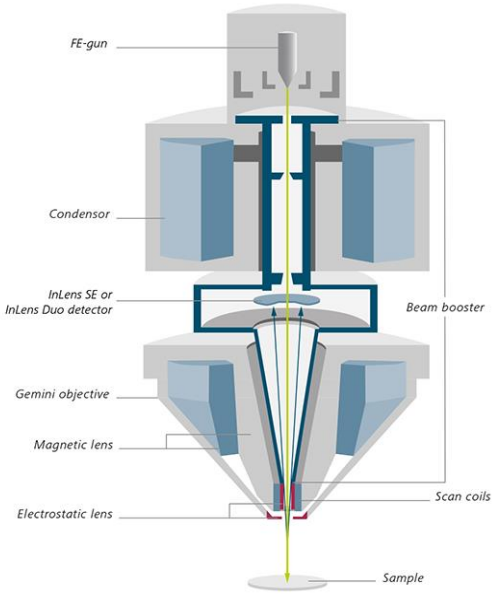

Figure 3.7: Schematic of Field Emission Scanning Electron Microscope [4].

The topography of CNSs in the present work was observed with *Carl Zeiss Merlin Compact* at 20kV. The samples were prepared on glass slides (1×1 cm) and carbon tape was applied on one side with marking on other side. The samples were dried by using a lamp to remove the moisture of the sample. The sample was gold coated after they dried

completely. CNSs with size 150-40nm were observed in high magnification images of FE-SEM.

3.3.4. High Resolution Transmission Electron Microscope (TEM/HR-TEM)

In transmission electron microscope transmission mode of electron imaging is utilized to find out the features inside the material. The sample characterized from TEM is most often an ultrathin section less than 100 nm thick. Transmission electron microscopes are capable to give images at high resolution than other microscopes, due to the smaller de Broglie wavelength of electrons. A high energy beam is passed through a sample and the interaction between the atoms and electrons can be used to observe crystal structure, dislocations and grain boundaries in the structure. A schematic diagram of Transmission electron microscope is shown in figure 3.8.

In the present study the samples were prepared on Cu grids for TEM analysis. One drop of each sample was dropped on the grid and then dried under lamp to remove the moisture. *Jeol 2100f* transmission electron microscope of high resolution at 20kV was used to analyze CNSs.

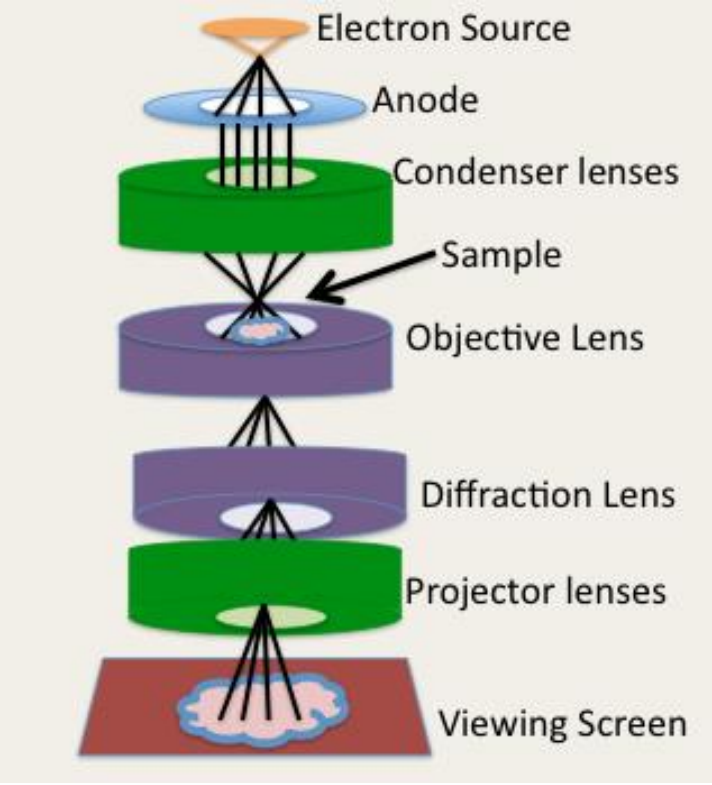

Figure 3.8: Schematic of Transmission Electron Microscope [5].

3.3.5. Ultraviolet Visible (UV-Vis) Spectroscopy:

The optical properties of CNSs are investigated from UV-VIS spectroscopy. It uses light in the visible, ultraviolet and near infrared ranges. It requires the spectroscopy of photons in the UV-Visible region. In this region of the electromagnetic spectrum, particles undergo electronic transition from excited state to ground state, while absorption transition from ground state to excited state. It measures transmittance or absorption of a sample as a function of wavelength when light of certain intensity and frequency range is passed through the sample.

1) The band gap energy, $E = h\,c/\lambda$
2) Band gap can be calculated by Tauc method [6]

$$\alpha h\nu = B^2 (h\nu - E_g)^n \qquad (3.2)$$

Where, $h\nu$ = photon energy

α= absorption coefficient

E_g= band gap of the material

n = 2, 1/2, 2/3 and 1/3 for direct allowed, indirect allowed, direct forbidden and indirect forbidden transitions respectively. UV-Visible spectrometer is shown in figure 3.9.

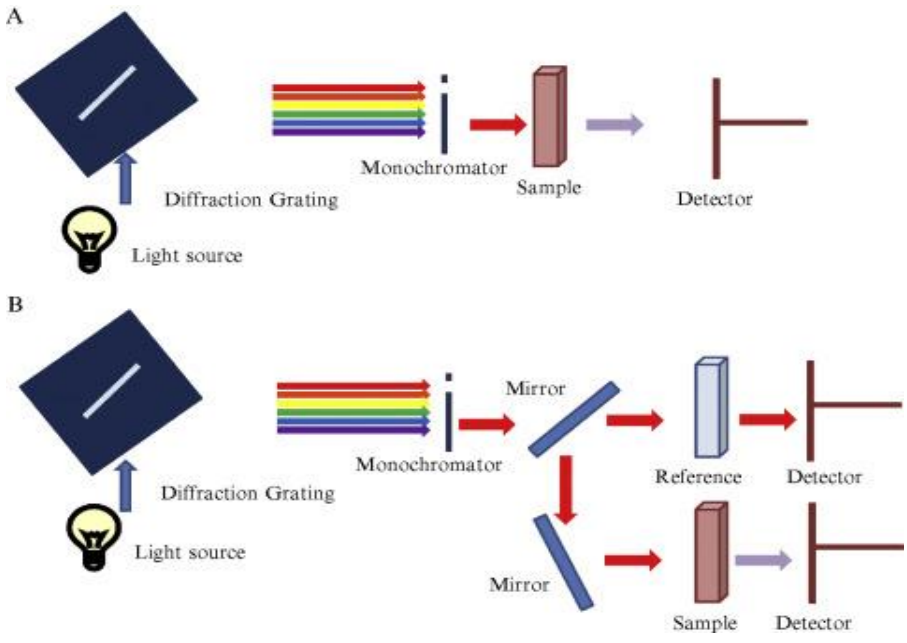

Figure 3.9: UV-Visible spectrophotometer setup [7].

In the present work the data was analyzed to calculate the band gap of CNSs. The absorption spectra for CNSs in solution was recorded at room temperature with *Hitachi U-3900H* spectrometer in the wavelength range of 200-800 nm.

3.3.6. Fourier Transform Infrared Spectroscopy (FT-IR):

IR spectrum is an analytical tool to identify the functional groups of a particular compound and to excess the purity of a sample. It is the measurement of absorption of different frequencies by a sample placed in the path of an IR beam. It provides spectrum with a large number of absorption bands and gives the information about the structure of a particular compound. The IR spectrum is generally presented by wave number on the x-axis and percent transmittance on y-axis. A simple optical layout of FTIR spectrometer is shown in figure 3.10.

In the present study the presence of different bonds on the surface of CNSs was analyzed by *Spectrum 400 FTIR* spectrometer for CNSs solution in 650-4000 cm^{-1}.

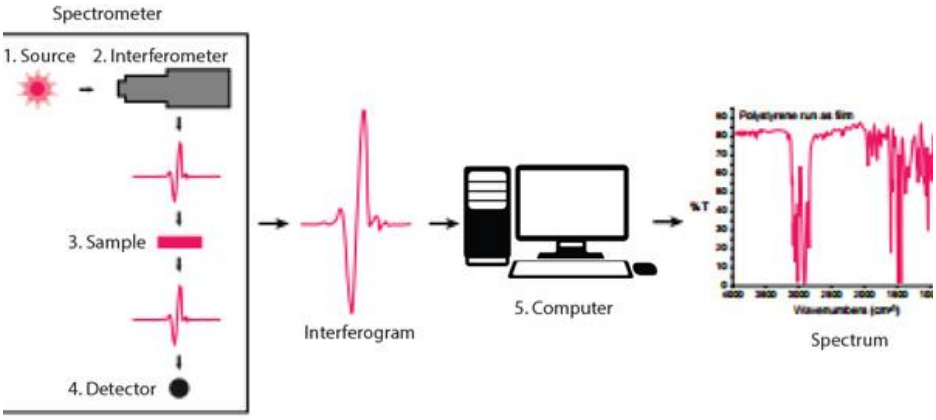

Figure 3.10: Schematic illustration of FTIR system [8].

3.3.7. Dynamic Light Scattering (DLS):

Dynamic light scattering studies the properties of inhomogeneous and dynamic media. This technique is used to determine the size and size distribution profile of small particles in the submicron region. When light hits the particles it scatters in all directions. Then the suspended particles exhibit brownian motion and the velocity distribution of particles determines the particle size. A schematic diagram showing the scattering of laser from particles is shown in figure 3.11.

The size distribution of CNSs was analyzed with *Brook heaven 90 plus* particle size analyzer for CNSs in solution.

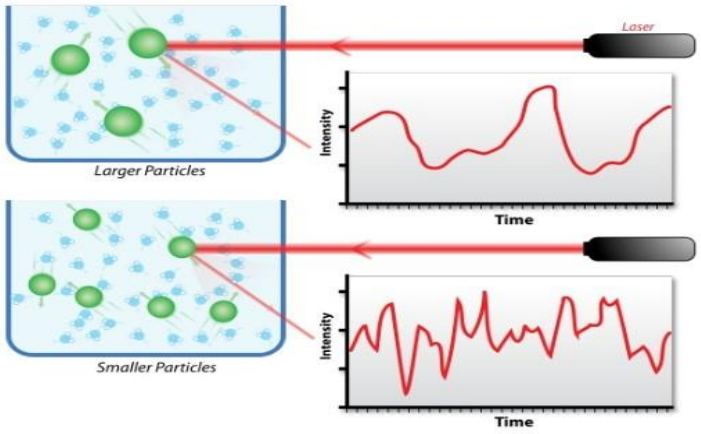

Figure 3.11: Schematic of Dynamic Light Scattering [9].

3.3.8. Thermo gravimetric (TG) Analysis:

The properties of a material change with temperature and the thermal stability of the material can be observed from thermogravimetry. Thermal analysis can also be used to study the heat transfer through the structures or temperature difference between a sample and a reference material. To calculate the mass loss of a sample with temperature, the mass of an unknown material is compared with a standard mass by comparing their weights in TGA. The measurements are taken in air or under an inert gas (N_2 or H_2). Figure 3.12 shows the schematic of thermo gravimetric analysis.

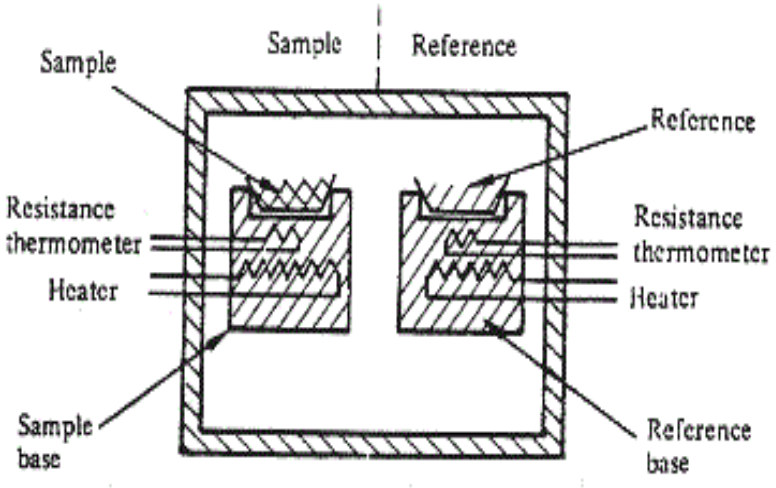

Figure 3.12: Thermo gravimetric Analysis [10].

In the present study the thermal stability of the sample was characterized by *SDT METTLER TOLEDO* DSC-TGA. The measurements were taken in the presence of air at 10˚/min. The temperature range was taken from room temperature to 1000˚C.

3.3.9. Energy dispersive X-ray spectroscopy (EDX):

EDX is an analytical technique which is used to estimate the amount of an element in the sample. A beam of electrons or X-rays is focussed on the sample and this energy of X-rays from the sample is measured by EDX. This energy is the difference between the two shells and the atomic structure of the element. Hence the composition of the element can be measured from EDX.

In the present work the elements were analyzed by *OXFORD INCA x-act* instrument. The sample was prepared on a brass stub. The sample was dropped on the stub and then dried under a lamp to completely remove the moisture of the sample. The sample was gold coated and then EDX analysis was done to find the composition of elements.

3.3.10. Inductively Coupled Plasma Mass Spectrometry (ICP):

An inductively coupled plasma mass spectrometry includes a high temperature ICP source and a mass spectrometer. This ICP source changes the elements to ions in the sample and these ions are detected by the mass spectrometer.

In the present study the concentration of iron was determined by *LEEMAN Prodigy XP ICP*. The sample was digested in aqua regia and the measurements were taken at room temperature.

3.3.11. Photo Catalytic Activity:

Photo catalysis is an ability of a nano material to accelerate a photo reaction as a catalyst in the presence of light (Ultraviolet light, sunlight). Photo catalytic activity depends on the capability of the catalyst to create electron-hole pairs. It generates free radicals to undergo secondary reactions. This technique has been investigated for the degradation of methylene blue (MB) dye as a metal organic contaminant under UV-Vis light irradiation.

In our present investigation the experiments were done in a photo reactor having a cylindrical glass vessel in the presence of UV and visible light source. A 0.005 gm of CNSs as the catalyst was dissolved in the 100ml of the MB dye solution (0.0001 gm). Prior to the UV light radiation the reaction mixture was stirred for 30 min in the dark for the adsorption-desorption equilibrium between the dye solution and the catalyst.

Then the mixture was activated under the UV light source. After specific intervals of time, 4ml sample solution was taken from the bulk solution and the dye solution was separated out from the catalyst by using a 4000 rpm centrifuge. The absorption spectrum of MB solution was recorded by UV-Vis spectrophotometer at wavelength 664 nm during the photo degradation process.

References

1. M. H. Joula, M. Farbod, Appl. Surf. Sci. **347** (2015) 535-540.
2. B.E. Warren, XRD, Classic X-ray Physics, General Publishing Company (1990).
3. P. W. Hawkes, L. Reimer, SEM Physics of image formation and micro analysis, springer (1985).
4. N. Brodusch, H. Demers, R. Gauvin, FE-SEM new perspectives for materials characterization, Springer Singapor (2017).
5. D.B. Williams, C.B. Carter, Transmission electron microscope, Springer science (2009).
6. M. Mahajan, G. Singla, K. Singh, O.P. Pandey, J. solid state chem. **232** (2015) 108-117.
7. H.H. Perkampus, UV spectroscopy and its applications, Springer (1992).
8. B. C. Smith, Fundamentals of FTIR spectroscopy, CRC Press (1996).
9. B. J. Berne, R. Pecora, DLS with applications, Dover Publications, Inc. Mineola New York (2000).
10. J. Russell, R. Cohn, Thermo gravimetric analysis, Book on demand (2012).

CHAPTER 4

RESULTS AND DISCUSSION

In this chapter, the characterization results for the carbon nanospheres (CNSs) synthesized from various polysaccharides have been presented.

4.1 Sample synthesis optimization

The synthesis conditions for obtaining the uniform and mono-disperse CNSs from saccharides were optimized by varying the synthesis time at the constant concentration of 0.1mol/l sucrose. Figure 4.1 shows the SEM images for the samples obtained. The results obtained from the analysis of SEM images are listed in table 4.1. From this data it is clear that in present setup the mono-dispersed samples are obtained for heating at 180˚C for 8 hrs.

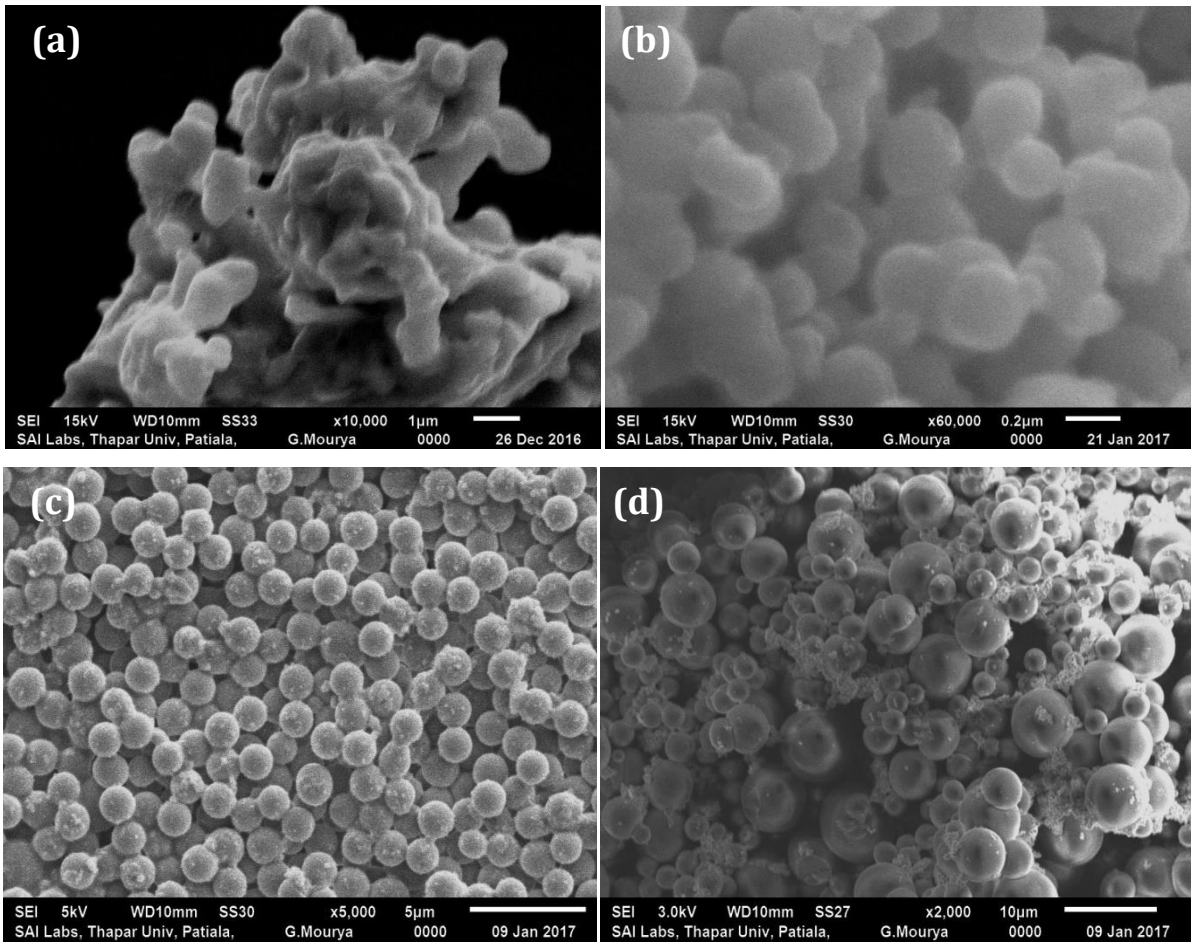

Figure 4.1: SEM images showing the effect of synthesis time on the obtained product. (a) 1 h, (b) 5 h, (c) 8 h, (d) 18 h

Table 4.1: Details of CNSs samples obtained for different synthesis times.

Sample name	Time (h)	Size
01 h	1	0.7-1.05 µm
05 h	5	0.2-0.3 µm
08 h	8	1.5 µm
18 h	18	2.5-5 µm

4.2 Mono-dispersed CNSs synthesis from sucrose

The crystal structure and the phases present in the synthesized CNSs were characterized by XRD. A representative XRD pattern for CNSs is shown in figure 4.2. The broad peak at angle 40^0 represents the amorphous structure of CNSs. Such amorphous structures have also been obtained in previous studies because of low crystallization in the samples [1-2].

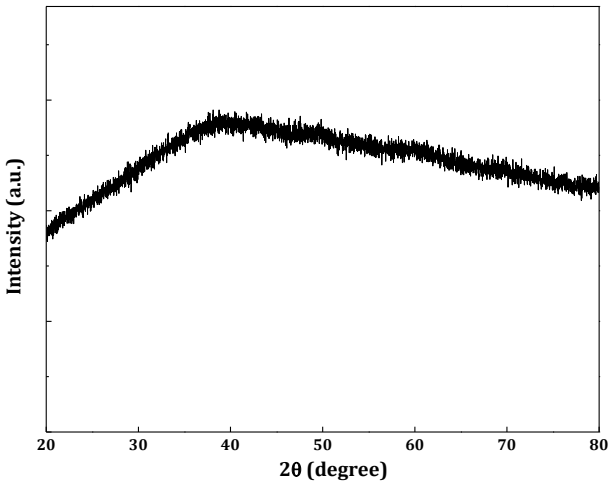

Figure 4.2: XRD pattern of synthesized CNSs (sample SC04).

The uniform and mono-disperse CNSs were synthesised from different concentration sucrose solutions (0.1-0.0025 mol/l) to know the variation of CNSs size with parent solution concentration. Figure 4.3 shows the SEM/FE-SEM images for the synthesized samples. The images clearly show the smooth surface, uniform size and spherical morphology of the synthesized samples.

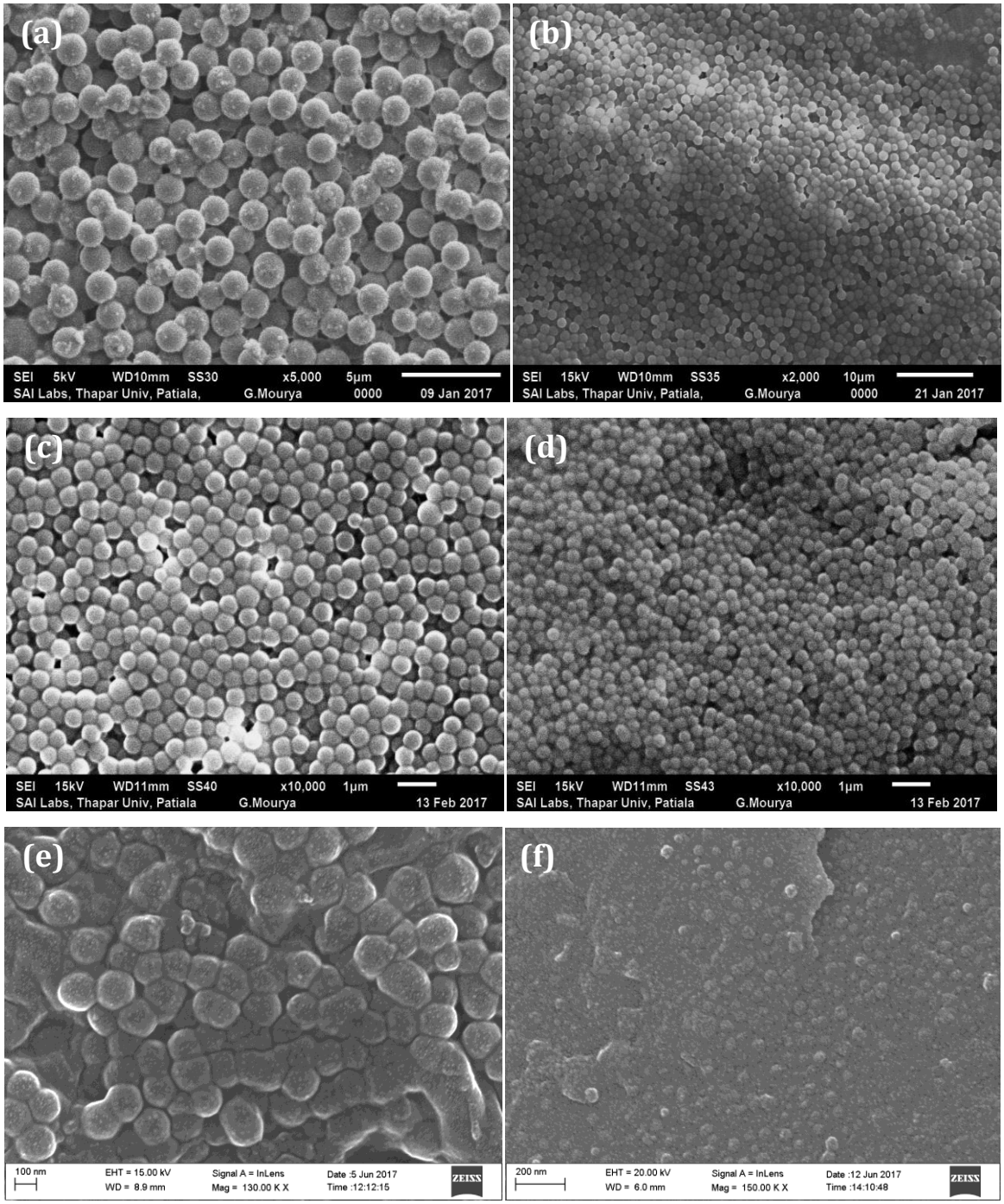

Figure 4.3: SEM/FE-SEM images of CNSs showing uniform and spherical morphology of CNSs for SC01, SC02, SC03, SC04, SC05 and SC06 (a-f).

The detailed particle size analysis of the synthesized samples was done from SEM/FE-SEM images with AxioVision LE64 software. Nearly 100 particles from different areas of different images were analysed. The analysis shows that the particle

size follows narrow sized log-normal distribution (Figure 4.4 (a)). The log-normal probability distribution was calculated by using the following equations [3]:

$$f(d) = \frac{1}{\sqrt{2\pi} d_i log \sigma_g} \exp\left\{-\frac{(log\, d_i - log\, \mu_g)^2}{2\,(log\, \sigma_g)}\right\} \quad (4.1)$$

$$\log \sigma_{g=} \sqrt{\frac{\sum(\log d_i - \log \mu_g)^2}{\sum n_i}} \quad (4.2)$$

$$\log \mu_g = \frac{\sum \log d_i}{\sum n_i} \quad (4.3)$$

Where,

f(d) denotes the log-normal distribution, d_i the diameter of particle, n_i the number of particles with diameter d_i, log μ_g the mean diameter and σ_g is the geometrical standard deviation, respectively.

Table 4.2 lists the average CNS size obtained from the log-normal distribution graphs. As expected, Figure 4.4(b) shows the variation of CNSs size with parent solution concentration. The size of the CNSs decreases with solution concentration and low concentration shows a sharp decrease in CNSs size.

Table 4.2: Details of monodispersed CNSs samples synthesized in present study. All the samples have been obtained by soaking the autoclave for 8 h at 180 °C.

Sample Name	Name of saccharide	Concentration (mol/l)	Size	Band Gap (eV)
SC01	Sucrose	0.1	1.4 µm	2.2
SC02	Sucrose	0.05	1.1 µm	2.2
SC03	Sucrose	0.025	0.5µm	2.3
SC04	Sucrose	0.01	0.28 µm	2.8
SC05	Sucrose	0.005	163nm	2.8
SC06	Sucrose	0.0025	35 nm	3.3
GL01	Glucose	0.005	36 nm	3.3
XL01	xylose	0.005	15 nm	3.3

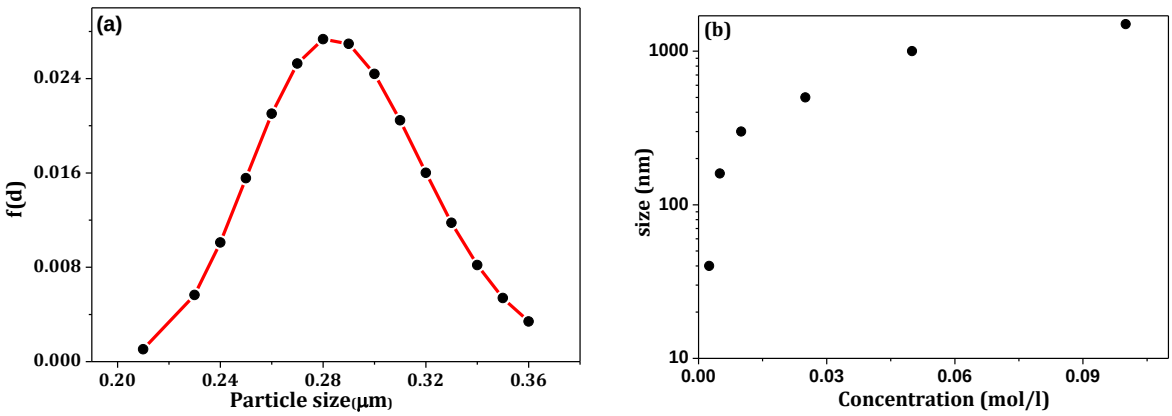

Figure 4.4: (a) Particle size distribution of SC04 sample. (b) Particle size variation of CNSs with concentration. (Y-axis of the graph has been plotted in log to show the small size data clearly)

Figure 4.5 shows the representative TEM and HR-TEM images for the CNSs synthesized from sucrose (SC05 Sample). HR-TEM image shows fringes which are 0.33 nm apart. These correspond with the {006} plane for hexagonal carbon (ICDD no.: 00-026-1076)

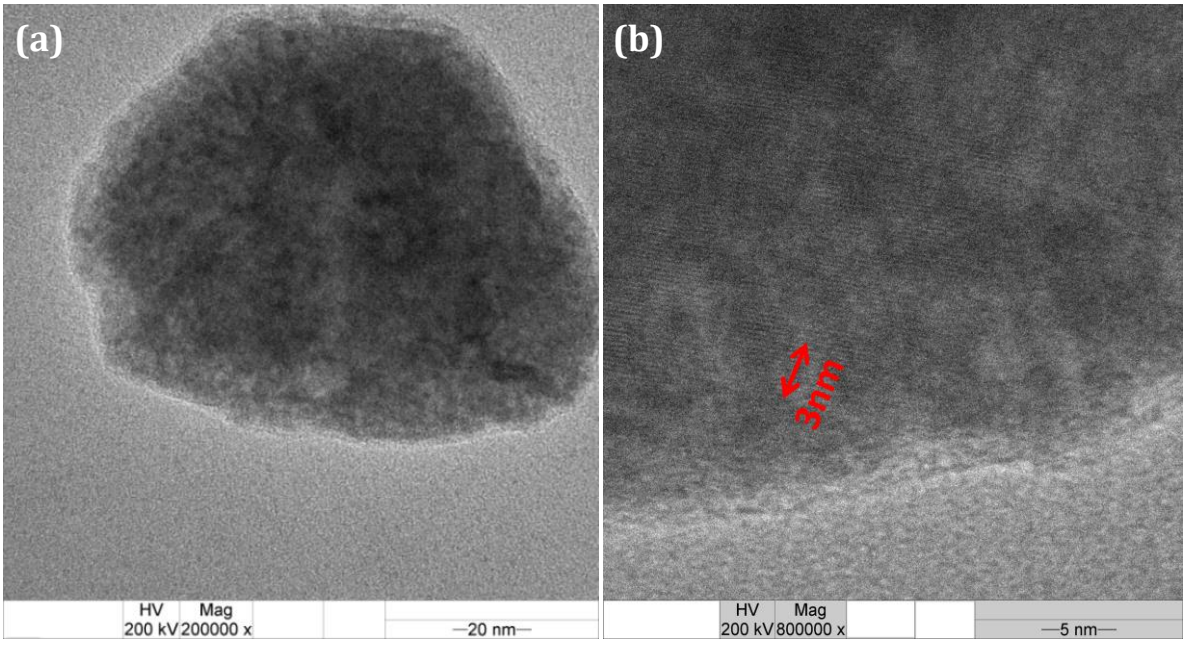

Figure 4.5: (a) TEM image for single CNS and (b) HR-TEM image for CNS showing {006} plane.

The optical properties of the synthesized CNSs were characterized by UV-Vis spectroscopy. Figure 4.6 (a) shows the representative graph for the UV-Vis data obtained for the CNSs samples. The synthesized samples show direct band gap. The band gap values have been calculated using the Tauc-plot and are listed in table 4.2. Figure 4.6 (b) shows the representative Tauc plot for the CNSs samples.

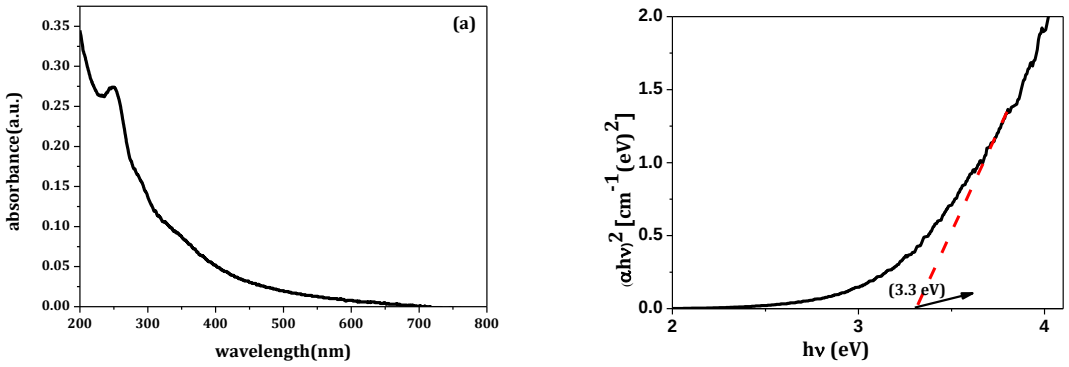

Figure 4.6: (a) The UV-Vis data obtained for the GL04 (b) Tauc plot for GL04.

The functional groups in CNSPs were investigated by FT-IR spectroscopy. The FT-IR spectra of SC05, GL01 and XL01 CNSPs have been shown in figure 4.7.

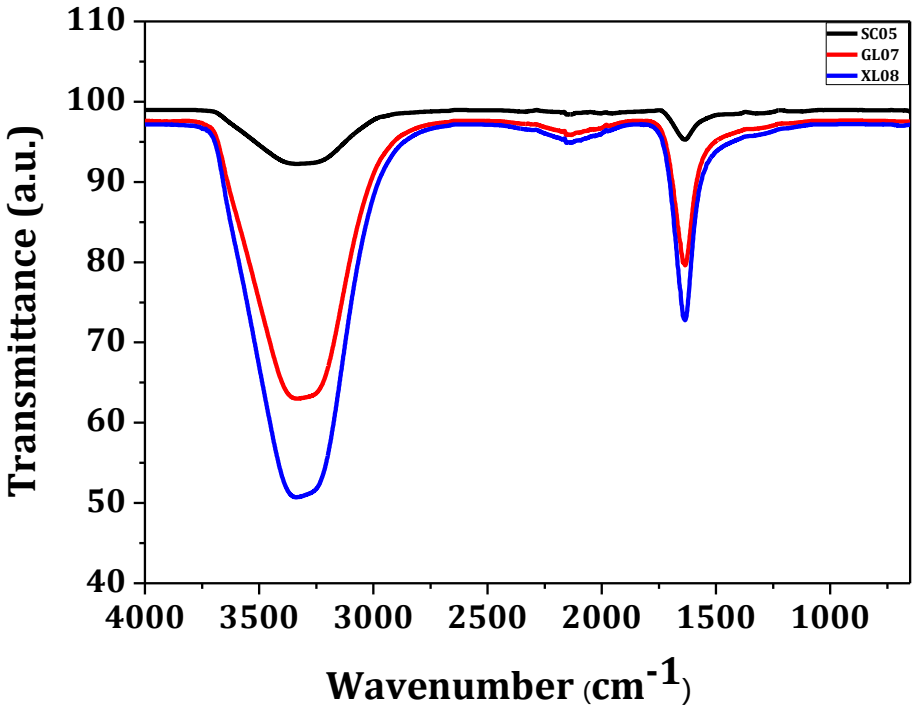

Figure 4.7: FT-IR spectra of synthesized CNSs for SC05, GL01 and XL01.

The position of different IR peaks and the corresponding functional group are mentioned in the table 4.3.

Table 4.3: represents the IR peak and the corresponding functional group.

Peak	Bond
3308-3338 cm^{-1}	-OH
1635.76 cm^{-1}	C=C

4.3 Effect of saccharide

The effect of saccharide variation on the synthesized CNSs is checked by using replacing the sucrose in the starting solution with glucose and xylose (Table 4.2). The CNSs obtained were compared with those obtained for the same concentration of sucrose. TEM and FE-SEM images of the synthesized CNSs for glucose and xylose have been shown in figure 4.8 and 4.9.

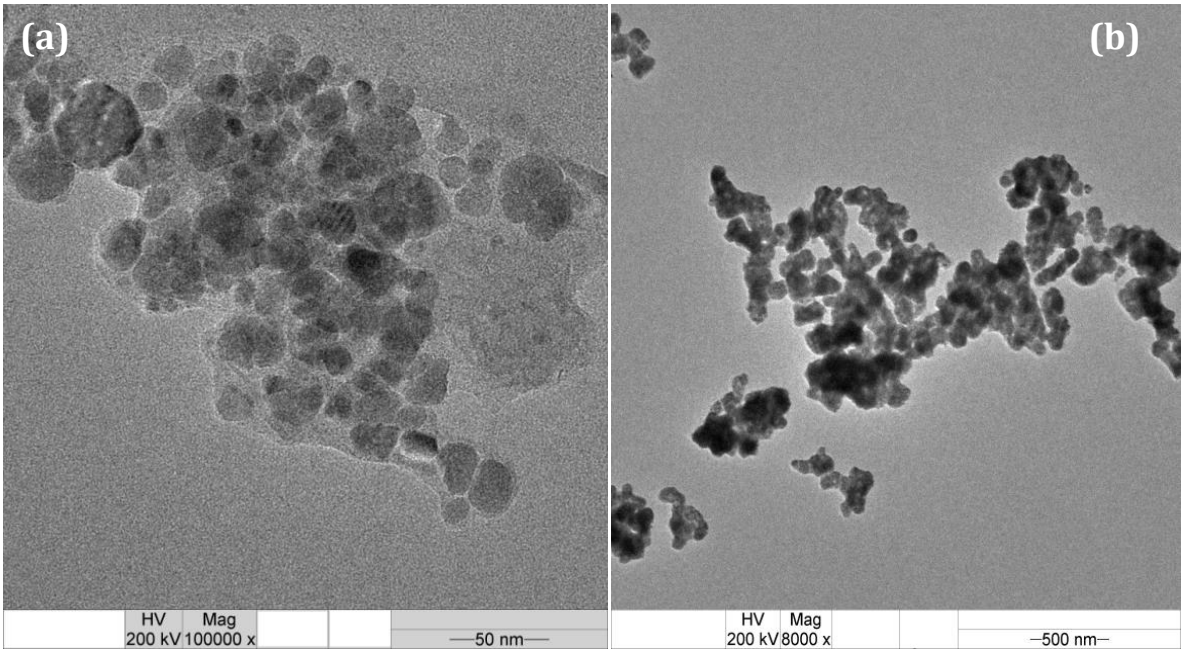

Figure 4.8: (a-b) TEM images of CNSs of GL01 and XL01

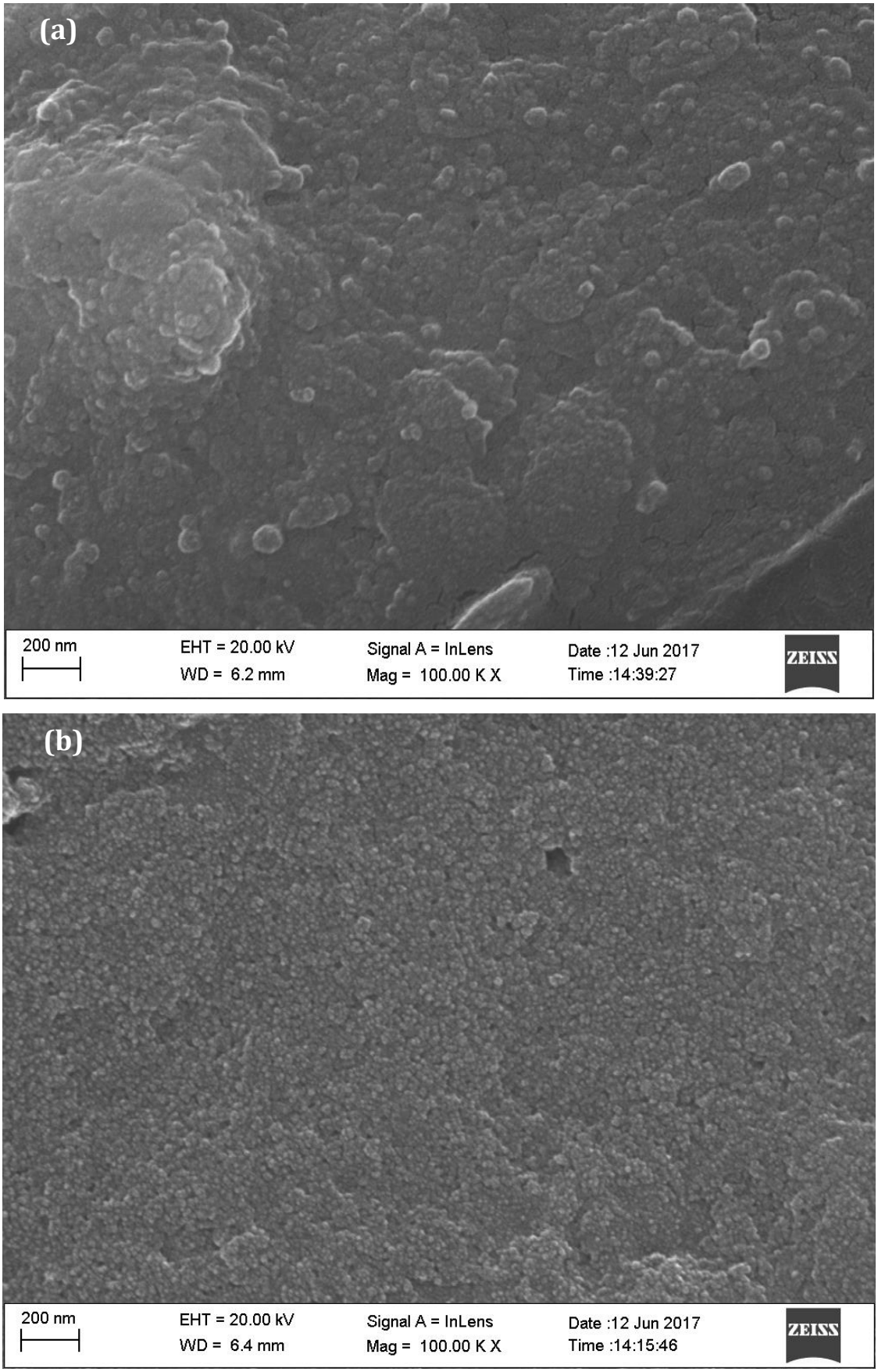

Figure 4.9: (a-b) FE-SEM images of CNSs of GL01 and XL01.

From the analysis, it was observed that for the same concentration the size of CNS varies as Sucrose (163nm)>Glucose (36nm) >Xylose (15nm) (figure 4.10). This variation occurs due to the difference in decomposition products of the respective saccharides [4].

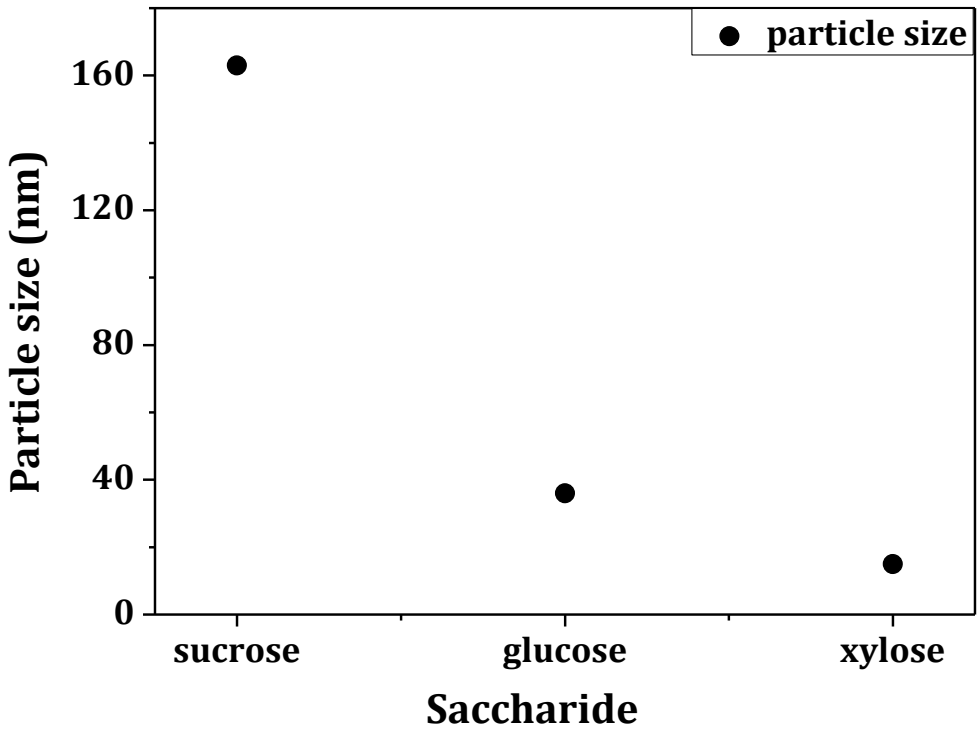

Figure 4.10: Particle size variation of CNSs with saccharides.

4.4 Study of size distribution profile in the solution

The size of CNSs in solution was analysed by Dynamic light scattering (DLS).The representative particle distribution graph of CNSs as obtained from DLS has been shown in Figure 4.11. The data obtained for all the samples has been summarized in table 4.4.

Comparing the data obtained from DLS (table 4.4) and SEM (table 4.2), it is observed that the size distribution of CNSs for GL01 and XL01 from DLS is very large due to increased agglomeration of CNSs.

Table 4.4: represents the concentration and size distribution of various samples.

Sample Name	Concentration (mol/l)	Size (nm)
SC01	0.1	637
SC03	0.025	525
SC04	0.01	316
SC05	0.005	239
SC06	0.0025	174
GL01	0.005	845
GL02	0.01	250
XL01	0.005	4563
XL02	0.01	249

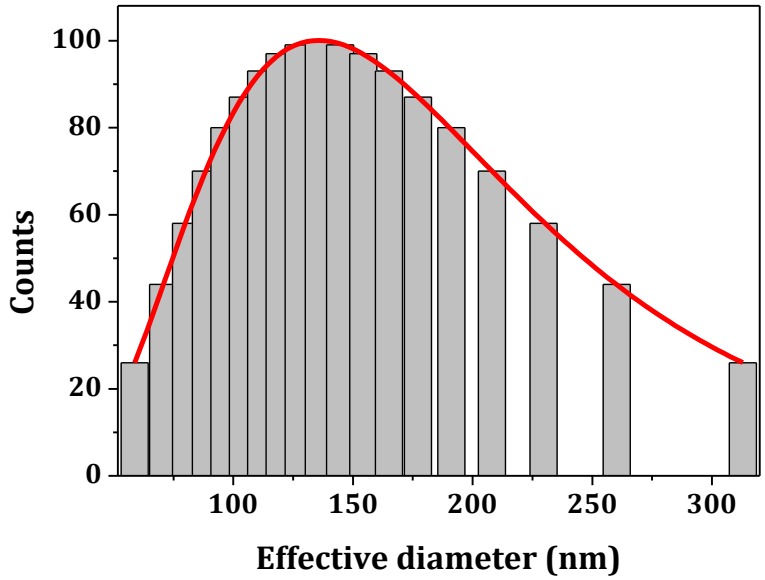

Figure 4.11: Particle size distribution graph for SC05.

4.5 TG analysis

The thermal stability of synthesized CNSs was analysed using TG. Figure 4.12 gives the TG plot for the SC04 sample. The initial weight loss of 8% which starts at 100 °C is due to removal of water and other adsorbed species from the surface of the CNSs. Above 200 ˚C there is an increase in the slope of the TG curve and a continuous weight loss till 500 °C with nearly 50% weight loss. This continuous weight loss is a signature of the

oxidation of dangling bonds present on the surface of the CNSs. The extended amount of weight loss indicates that at temperatures above 200 ˚C the CNSs are being degraded due to the fraying of the constituent graphitic sheets. The stabilization at around 550 °C indicates that the inner core of the CNSs is quite stable. And the breakdown of this core takes place at around 630 °C which results in complete destruction of the CNSs. TG data clearly shows that the CNSs in the synthesized samples are consisting of loosely wound graphitic layers with a strong inner core [5-7].

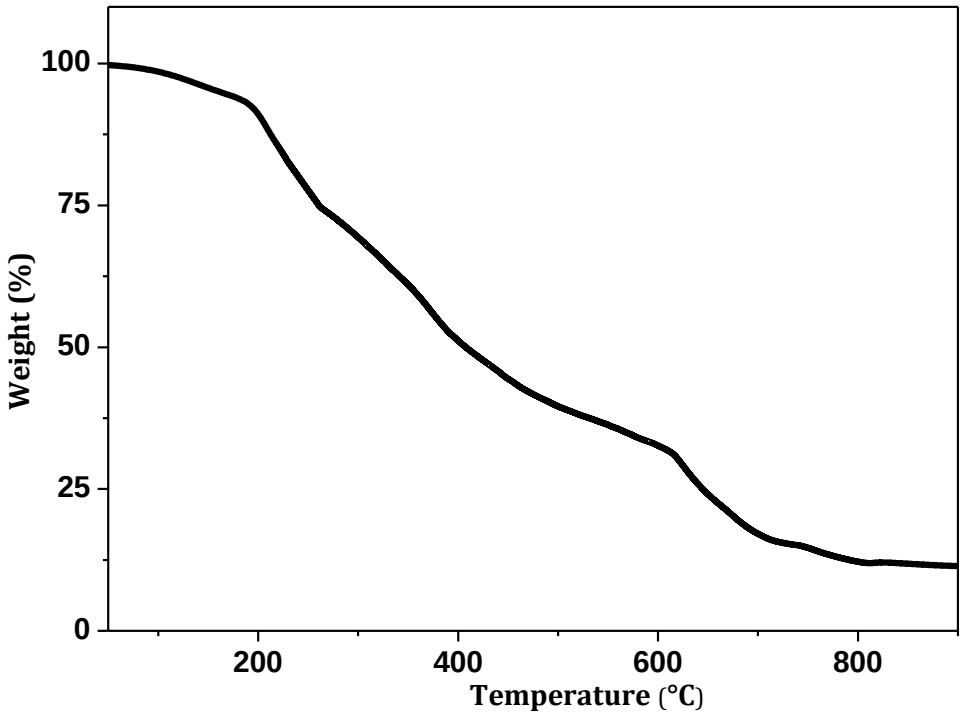

Figure 4.12: TG plot of synthesized CNSs for SC04.

The stabilization of TG data at 11% at high temperatures clearly indicates that the synthesized CNSs solution contains a non-volatile impurity.

4.6 Determination of impurity in CNSs samples:

The ICP analysis of the CNS dissolved in aqua regia shows the presence of 10ppm Fe in 25mg SC04 sample. The presence of Fe was also confirmed by EDAX (figure 4.13).

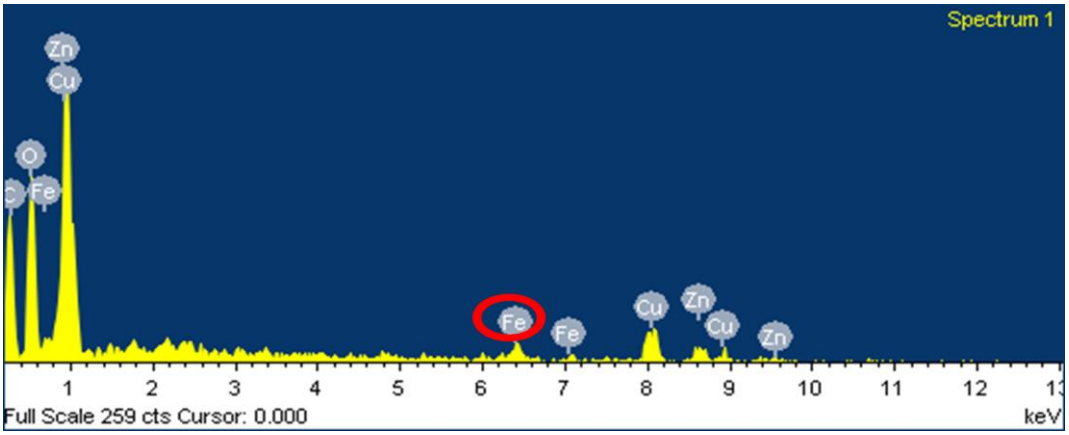

Figure 4.13: EDAX spectrum of CNS of SC04

4.7 Photo-catalytic Activity

The band gap calculations (table 4.2) show the synthesized CNSs have a direct band gap of value < 3.3eV [8]. This renders the samples as a suitable candidate for photo-catalysis under UV and Visible spectra.

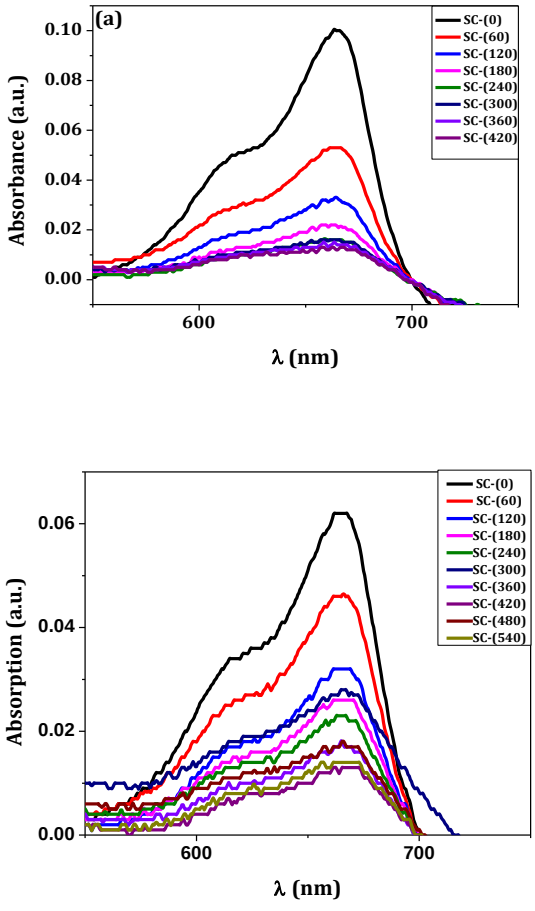

Figure 4.14: Absorption spectra of degradation of MB under (a) visible source (b) UV source

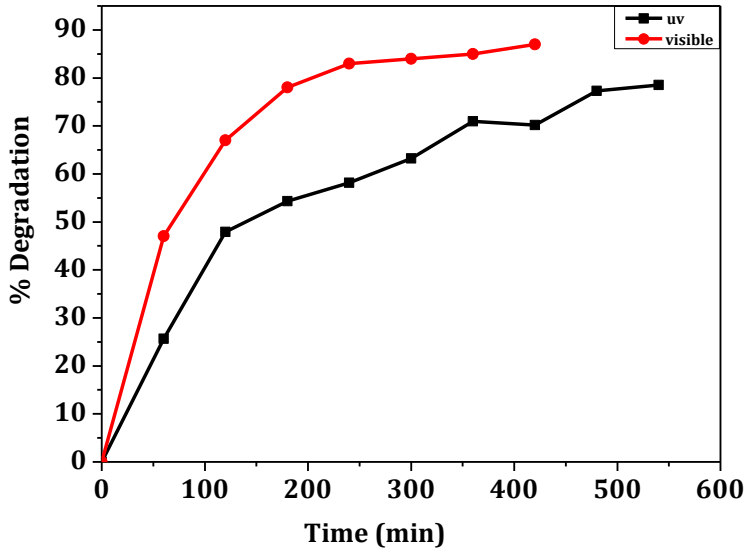

Figure 4.15: Degradation of MB with time in the presence of UV and Visible light.

The degradation of MB with time for UV and Visible source is shown in Figure 4.16. To calculate the degradation efficiency the following equation can be used [8]:

$$D(\%)=[(C_0-C_t)/C_0]\times 100 \qquad (3.4)$$

Where, C_0 and C_t represents the concentration of MB at time 0 and t respectively. The degradation efficiency of CNS for MB is 78% under UV light in 540min and 87% under visible light in 420min.

The higher degradation efficiency of CNS was obtained due to its spherical and nano size particles and dangling bonds at edges. The photo generated electrons lowers the molecular oxygen (O_2) into superoxide radicals and these radicals react with water molecule and form oxidizing radical species the interact with MB and degrades it.

These results clearly show that the synthesized CNS can be used as photo catalysts for organic waste materials.

References

1. Q. Wang, F. Cao, Q. Chen, C. Chen, Mater. Let. **59** (2005) 3738-3741.

2. H. Kristianto, C. D. Putra, A. A. Arie, M. Halim, J. K. Lee, Procedia chem. **16** (2015) 328-333.

3. A. Gupta, G. Singla, O.P. Pandey, Ceram. Int. **42** (2016) 13024-13034.

4. Q. Yan, R. Li, H. Toghiani, Z. Cai, J. L. Zhang., T. R. Energy **1** (2015) 119-128.

5. M. H. Joula, M. Farbod, Appl. Surf. Sci. **347** (2015) 535-540.

6. S. P. Dubey, A. D. Dwivedi, M. Sillanpaa, Y. kwon, C. Lee, RSC Adv. **4** (2014) 46114.

7. A. Nieto-Marquez, R. Romero, A. Romero, J. L. Valverde, J. Mater. Chem. **21** (2011) 1664-1672.

8. M. Mahajan, G. Singla, K. Singh, O.P. Pandey, J. solid state chem. **232**(2015) 108-117.

CHAPTER 5

CONCLUSIONS AND FUTURE SCOPE

5.1 Conclusions

The mono-dispersed carbon nanospheres (CNSs) using saccharide solutions were synthesized by hydrothermal process and then characterized by XRD, HRTEM, DLS, UV-Visible spectroscopy, FT-IR, SEM with EDS technique, VSM, ICP etc. Three saccharides namely, sucrose, xylose and glucose have been used in the present work. The size of the CNSs decreases with the saccharide solution concentration with smaller concentrations having more drastic effect. The CNSs produced from the present method typically have an average size in the range of 1500 – 15nm having smooth surfaces. Xylose gives the smallest CNSs. The CNSs were amorphous in nature. Samples show direct band gap which changes with the size of CNSs. This makes the synthesized samples viable for the photo catalytic applications in UV as well as visible region. The application of the synthesized CNSs as photo catalyst for organic waste degradation has been confirmed by degradation of methylene blue (MB) dye in the presence of UV and visible light. The degradation efficiency is more in visible light.

5.2 Future scope:

The TG indicated the presence of non-volatile impurity in the CNSs solution. ICP and EDAX confirmed the impurity as iron. To prevent the same in future the work should be carried out in lined autoclave. The effect of CNSs size on the degradation efficiency in photo catalytic experiments needs to be studied further.